DTIC FILE COPY

SECURITY CLASSIFICATION OF THIS PAGE

REPORT DOCUMENTATION PAGE

Form Approved OMB No. 0704-0188

1a. REPORT SECURITY CLASSIFICATION UNCLASSIFIED	1b. RESTRICTIVE MARKINGS NONE
AD-A217 649 S)	3. DISTRIBUTION/AVAILABILITY OF REPORT APPROVED FOR PUBLIC RELEASE; DISTRIBUTION UNLIMITED.
	5. MONITORING ORGANIZATION REPORT NUMBER(S) AFIT/CI/CIA-88-226
6a. NAME OF PERFORMING ORGANIZATION AFIT STUDENT AT JOHNS HOPKINS UNIVERSITY 6b. OFFICE SYMBOL (If applicable)	7a. NAME OF MONITORING ORGANIZATION AFIT/CIA
6c. ADDRESS (City, State, and ZIP Code)	7b. ADDRESS (City, State, and ZIP Code) Wright-Patterson AFB OH 45433-6583
8a. NAME OF FUNDING/SPONSORING ORGANIZATION 8b. OFFICE SYMBOL (If applicable)	9. PROCUREMENT INSTRUMENT IDENTIFICATION NUMBER
8c. ADDRESS (City, State, and ZIP Code)	10. SOURCE OF FUNDING NUMBERS PROGRAM ELEMENT NO. / PROJECT NO. / TASK NO. / WORK UNIT ACCESSION NO.

11. TITLE (Include Security Classification) (UNCLASSIFIED)
AN INVESTIGATION OF THE POTENTIAL OF 31-PHOSPHORUS NUCLEAR MAGNETIC RESONANCE SPECTROSCOPY TO PREDICT RADIATION SENSITIVITY

12. PERSONAL AUTHOR(S)
CINDY BOWSER

13a. TYPE OF REPORT	13b. TIME COVERED	14. DATE OF REPORT (Year, Month, Day)	15. PAGE COUNT
~~THESIS~~/DISSERTATION	FROM _____ TO _____	1988	106

16. SUPPLEMENTARY NOTATION
APPROVED FOR PUBLIC RELEASE IAW AFR 190-1
ERNEST A. HAYGOOD, 1st Lt, USAF
Executive Officer, Civilian Institution Programs

17. COSATI CODES			18. SUBJECT TERMS (Continue on reverse if necessary and identify by block number)
FIELD	GROUP	SUB-GROUP	

19. ABSTRACT (Continue on reverse if necessary and identify by block number)

90 02 01 005

20. DISTRIBUTION/AVAILABILITY OF ABSTRACT	21. ABSTRACT SECURITY CLASSIFICATION
☒ UNCLASSIFIED/UNLIMITED ☐ SAME AS RPT. ☐ DTIC USERS	UNCLASSIFIED
22a. NAME OF RESPONSIBLE INDIVIDUAL ERNEST A. HAYGOOD, 1st Lt, USAF	22b. TELEPHONE (Include Area Code) (513) 255-2259 / 22c. OFFICE SYMBOL AFIT/CI

DD Form 1473, JUN 86 *Previous editions are obsolete.* SECURITY CLASSIFICATION OF THIS PAGE

AFIT/CI "OVERPRINT"

AN INVESTIGATION OF THE POTENTIAL OF 31-PHOSPHORUS NUCLEAR MAGNETIC RESONANCE SPECTROSCOPY TO PREDICT RADIATION SENSITIVITY

by

Cindy Bowser

A dissertation submitted to The Johns Hopkins University in conformity with the requirements for the degree of Doctor of Philosophy

Baltimore, Maryland

1989

ABSTRACT

The ability of *in vivo* 31-Phosphorus Nuclear Magnetic Resonance (31-P NMR) Spectroscopy to predict radiation sensitivity following both single and fractionated therapy was evaluated in this study. For Radiation Induced Fibrosarcoma (RIF-1) tumors either, in their natural state or treated with the vasodilator, hydralazine, an increase in the ratio of phosphocreatine to inorganic phosphate (PCr/Pi) and tumor pH were shown to be significantly correlated ($p < 0.01$) with radiation sensitivity to a single dose of 15 Grays (Gy) of radiation. After administration of hydralazine to reduce tumor blood flow or flunarizine to increase tumor blood flow, time dependent changes were observed in the 31-P NMR spectrum. After hydralazine, there was a significant ($p < 0.01$) decrease in PCr/Pi over time. The opposite pattern was seen for flunarizine i.e., decline in Pi, and an increase in PCr and pH. The radiosensitivity of flunarizine treated tumors was substantially greater ($p < 0.05$) than that of hydralazine treated tumors.

Fractionated therapy (10 Gy + 10 Gy) at intervals of 0 to 72 hours was investigated. Significant changes were observed between the NMR spectra obtained before therapy and those obtained just prior to the second fraction. At eight and 16 hours after the first 10 Gy fraction a decline in Pi and a rise in tumor pH were observed. When the interval

between treatments was extended to 24 through 72 hours, a significant rise in the levels of phosphodiester compounds was observed compared to pre-treatment values. Histological analysis at 72 hours showed a significant increase of the necrotic fraction in the treated tumor as compared to the untreated tumor.

A slight ($p < 0.10$) improvement in therapy outcome was obtained when the second fraction was delivered at 16 hours (lower Pi, elevated pH).

When NMR parameters were compared to treatment outcome on an <u>individual</u> animal basis, values for the ratio of PCr to B-Nucleotide Triphosphate (both before treatment and before second fraction) were significantly correlated ($r = -0.39$, $p < 0.01$) with radiation sensitivity.

It appears that the results of 31-P NMR Spectroscopy are a significant but not strong predictor of radiation sensitivity in both single and fractionated radiation therapy.

DEDICATION

To my beautiful, life-long friends;

Thanks again, Mom and Dad.

ACKNOWLEDGMENTS

A Faithful Friend is a Source of Strength
and He Who has Found Such a Friend has Found a Treasure.

My Treasure Chest of Friends at Johns Hopkins has Included:

Dr. Janna Wehrle
Dr. Thomas Mitchell
Dr. Jerry Glickson
Dr. Ioannis Constantinidis
Dr. Alan Gittelsohn
Dr. James Anderson
Dr. Larry Dillehay
Dr. Grant Steen
Ms. Penny Jenkins
Ms. Lorraine Avinante
Ms. Joann DonDero
Ms. Cindy Martin
Mr. Gary Cromwell

This research was supported by both the National Cancer Institue through Grant No. 1 PO1 CA44703 awarded to Dr. Jerry Glickson and the United States Air Force, Air Force Institute of Technology.

TABLE OF CONTENTS

LIST OF ILLUSTRATIONS

LIST OF TABLES

I. INTRODUCTION

Sensitization of cells to radiation by oxygen has been recognized for 60 years, and it has been 30 years since Thomlinson and Gray found that the anatomy of human bronchial carcinomas suggests the presence of regions of hypoxic cells. These hypoxic cells may be responsible for local control failure in radiotherapy of human tumors, although this has not been conclusively demonstrated. It is known that even within the same tumor class, individual patients differ dramatically in their response to radiotherapy. Noninvasive Nuclear Magnetic Resonance (NMR) measurements of tumor oxygenation status could prove useful in predicting response to therapy. Tumors differ not only with respect to the fraction of radiobiologically hypoxic cells before treatment, but also with respect to the degree and time course of reoxygenation after single dose or fractionated therapy (1). The level of oxygenation measured by NMR techniques after treatment with radiation may be useful for improving fractionation schedules. This may be extremely important in rapidly growing tumors such as Burkitt's lymphoma, where cell proliferation during the treatment period appears to limit the effectiveness of radiotherapy (2).

During growth, tumors exhibit gradual 31-Phosphorus NMR spectral changes which qualitatively resemble those associated with hypoxia in normal tissue of the same type.

The concentrations of nucleotide triphosphates (NTPs) and phosphocreatine (PCr) decrease with time, while Pi (inorganic phosphate) increases. These observations suggested the usefulness of determining the state of perfusion and oxygenation of tumors by 31-P NMR spectroscopy (3). Well-oxygenated tumors are more sensitive to low linear energy transfer (LET) radiation than are hypoxic tumors, because oxygen is required to fix cytotoxic radicals. NMR may provide a noninvasive method for predicting tumor response to radiation, given the assumption that the state of tissue oxygenation may be determined by NMR spectroscopic techniques.

II. BACKGROUND

A. Nuclear Magnetic Resonance

The nuclei of certain nuclides, such as protium (1-H), or phosphorus (31-P), have unpaired nucleons and possess a property known as spin. This can be visualized as the nucleus revolving on its own axis (Figure 1a). Associated with the spin is a magnetic field, so that the nucleus can be regarded as polar. These nuclei and their fields are oriented randomly. If a stronger magnetic field is applied to a sample containing such nuclei, the nuclear "magnets" align along the field as a compass needle aligns along a magnetic field. Nuclei with spin obey the laws of quantum mechanics. Those nuclei which have a spin quantum number of I=1/2 (i.e., 1-H or 31-P) can have one of two orientations with respect to the applied field (Figure 1b). These two orientations result in nuclei with slightly different energies depending on their orientation, and the energy difference between the two states is proportional to the magnitude of the applied field. The number of nuclei in the lower energy state (oriented with the same direction as the applied field) is only slightly greater than those in the higher energy state (oriented opposite to the applied field). The ratio of the numbers is determined by the difference in energy between the two states, the magnetic field strength, and the temperature. For a sample with about 10^{23} nuclei, the difference in the population of

Figure 1

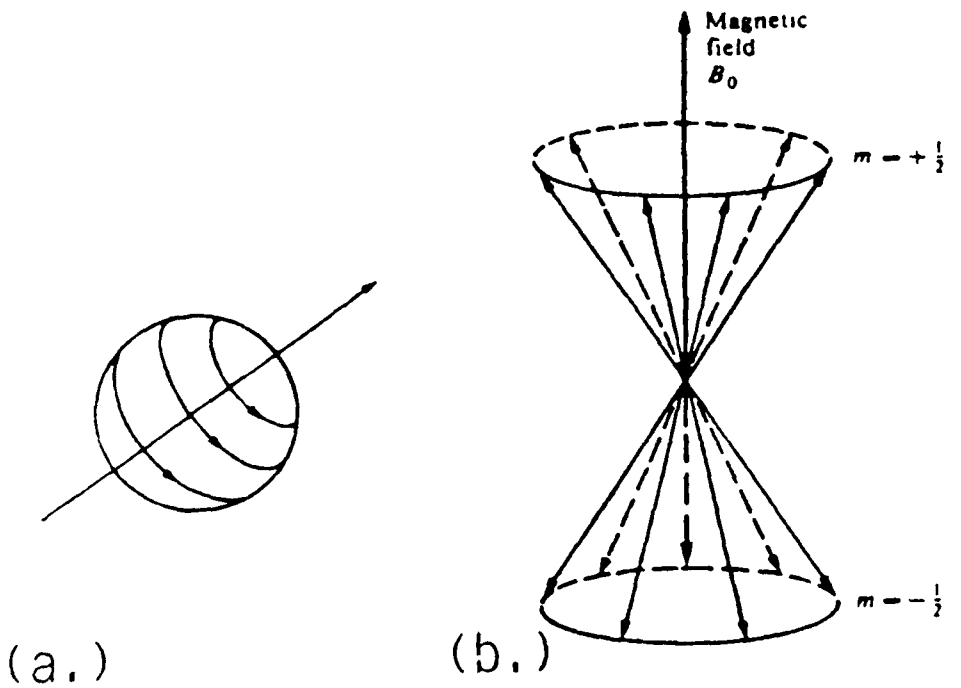

Models for Magnetic Spin

the two states would be about 10^{17} nuclei. Transitions between these states can be induced by applying an oscillating radio-frequency (rf) pulse of frequency, ν_o, that satisfies the equation, $\Delta E=h\nu$, where ΔE is the energy separation of the levels, h is Planck's constant (6.63×10^{-27}ergs-sec/Hz), and ν is frequency in hertz. The Larmor frequency, ν_o, is also related to the magnetic field strength by the following equation:

$$\nu_o = \frac{\gamma \, Bo}{2 \, \pi}$$

where Bo is the magnitude (in Tesla) of the first applied magnetic field. γ is known as the gyromagnetic ratio of the nucleus and varies from one nuclear isotope to another. The value of γ is 26.75 for 1-H and 10.83 for 31-P given in units of (x 10^{-7} radians/Tesla-second).

B. Nuclear Magnetic Resonance Spectroscopy

The resonance frequency of a nucleus is directly proportional to the local magnetic field experienced by the nucleus. In the preceding section we considered this field to be the applied field, Bo. If this were strictly true, every nucleus of a given nuclide would absorb energy at the same frequency. Instead, the applied field, Bo, also induces electronic currents in atoms and molecules, and these produce a further small field at the nucleus which is also proportional to Bo. The total effective field, Beff, at the nucleus is:

$$Beff = Bo\ (1-\sigma).$$

Therefore, ν_o becomes:

$$\nu_o = \frac{\gamma\ Bo}{2\ \pi}(1-\sigma)$$

σ is called the shielding or screening constant because the effect of these electronic currents is to shield the nucleus from the effects of the applied field. The magnitude of σ is dependent upon the environment of the nucleus, and therefore nuclei in different chemical environments give rise to signals at different frequencies. The separation of resonance frequencies from an arbitrarily chosen reference frequency is termed the "chemical shift". To eliminate the dependence of chemical shift on field strength, chemical shift is frequently given as a fraction of the reference resonance frequency in the dimensionless

unit of parts per million (ppm). The terms "upfield" and "downfield" are used to denote the direction of a chemical shift. Spectra are plotted according to the traditional rule of spectroscopy: decreasing frequency to the right. If one nucleus is more shielded than another, it will experience a reduced effective field and therefore resonate at a lower frequency; by convention it will have a more negative chemical shift, and will appear further towards the right-hand side of the spectrum.

The intensities of NMR signals, as measured from their areas, are proportional to the number of nuclei that contribute to them. The relative areas of the signals within a spectrum will be equal to the relative numbers, and hence concentrations, of the nuclei that contribute to them.

C. 1-H NMR Spectroscopy

The proton is the most sensitive nucleus for NMR spectroscopy (except 3-H, triton), however several features of the 1-H spectrum make it relatively difficult to analyze *in vivo*.

1. Its relatively narrow chemical shift range leads to poor resolution.

2. The presence of the large and relatively broad water solvent peak creates considerable difficulty when trying to observe the very much weaker signals from metabolities in tissue. Techniques for suppression of the water resonance *in vivo* are still imperfect.

3. In addition the resonances from the methyl and methylene groups of all the membrane lipids dominate another important region of the 1-H spectrum, where alanine and lactate resonate. The relatively high mobility of tumor lipids (4) causes lipid suppression techniques to work less well in tumors than in highly organized tissues such as brain.

4. A final problem is the inherent complexity of the 1-H spectrum due to the many different chemically distinct organic molecules of which hydrogen is a part. This is illustrated in Figure 2 which shows the spectrum of one relatively simple compound, glucose-6-phosphate.

These complex spectra can be utilized to provide information about the structure and mobility of molecules,

Figure 2

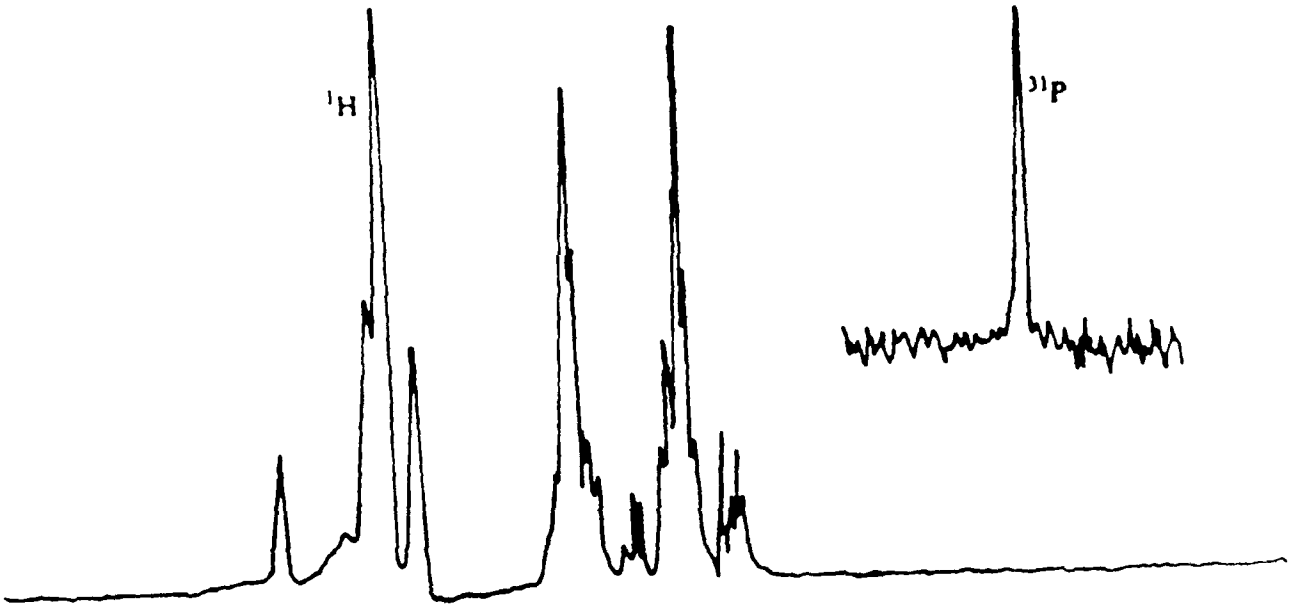

NMR Spectra of Glucose-6-Phosphate

however the *in vivo* system contains overlapping signals from so many compounds that interpretation of their spectra is difficult.

D. 31-P NMR Spectroscopy

The 31-P nucleus is particularly suitable for studies of living systems for several reasons:

1. Narrow resonant frequencies can be obtained, and they occupy a fairly wide range of chemical shifts leading to good spectral resolution at reasonable field strengths (i.e., greater than 2 Tesla). See Figure 3.

2. Although the sensitivity of detection for 31-P is only one-fifteenth that of 1-H, it is nevertheless one of the most sensitive nuclei. Phosphate metabolites free in solution at concentrations of 0.1 millimolar or greater are potentially detectable by in vivo 31-P NMR spectroscopy. Moreover, 31-P is the only naturally occurring isotope of phosphorus and so no isotopic enrichment of specimens is necessary.

3. The spectra are simple and easy to interpret.

4. Several important phosphorus-containing compounds (e.g., adenosine triphosphate [ATP], phosphocreatine [PCr], phosphomonoesters [PME], phosphodiesters [PDE] and inorganic phosphate [Pi]), occur in living systems at concentrations high enough (0.1 mM and above) to be detectable by 31-P NMR. Because of the involvement of these compounds in the energetics of living systems, 31-P NMR provides an ideal means of monitoring the energetic state of living cells, tissues and organs.

5. 31-P provides a method for measuring tissue pH.

Figure 3

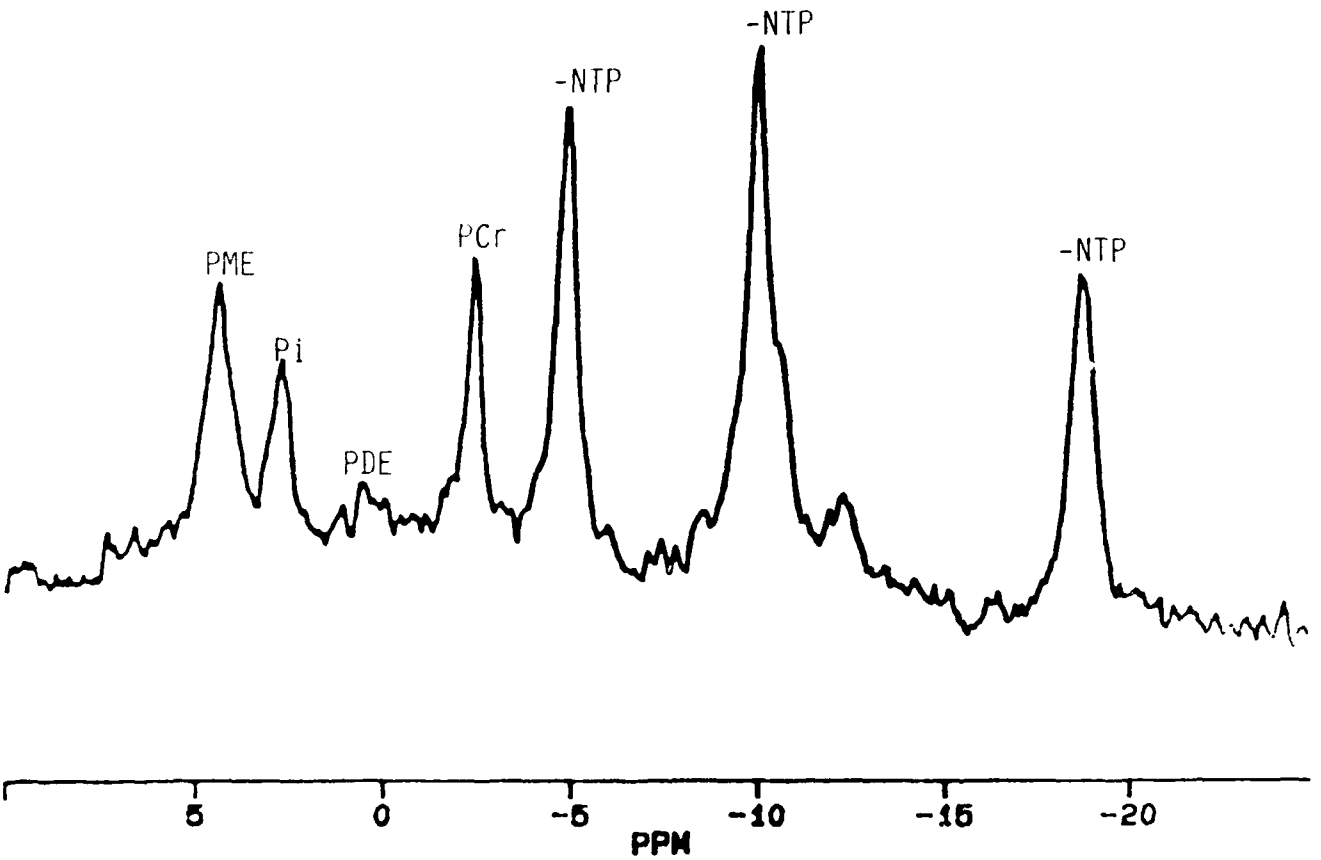

In Vivo 31-P NMk Spectra from a 9-L Gliosarcoma (8.5T)

The pH of many tissues provides a valuable guide to their metabolic state; this is because a decline in pH tends to reflect the production of lactic acid which accumulates under ischemic or hypoxic conditions. The resonance of inorganic phosphate is most commonly used because it is particularly sensitive to pH in the physiological pH range, and is readily observable in the majority of 31-P spectra.

Inorganic phosphate exists mainly as HPO_4^{-2} and $H_2PO_4^{-1}$ at physiological pH. In the absence of chemical exchange these two species would give rise to two resonant frequencies separated by about 2.4 ppm. In solution however, the two species exchange with each other very rapidly, and as a result the observed spectrum contains a single resonance, the frequency of which is determined by the relative amounts of the two species. The frequency of the signal measured as a function of pH produces a typical titration curve (Figure 4). Because of effects of ionic strength and the presence of divalent cations, Pi titration curves for biological systems are usually determined empirically in tissue homogenates.

Figure 4

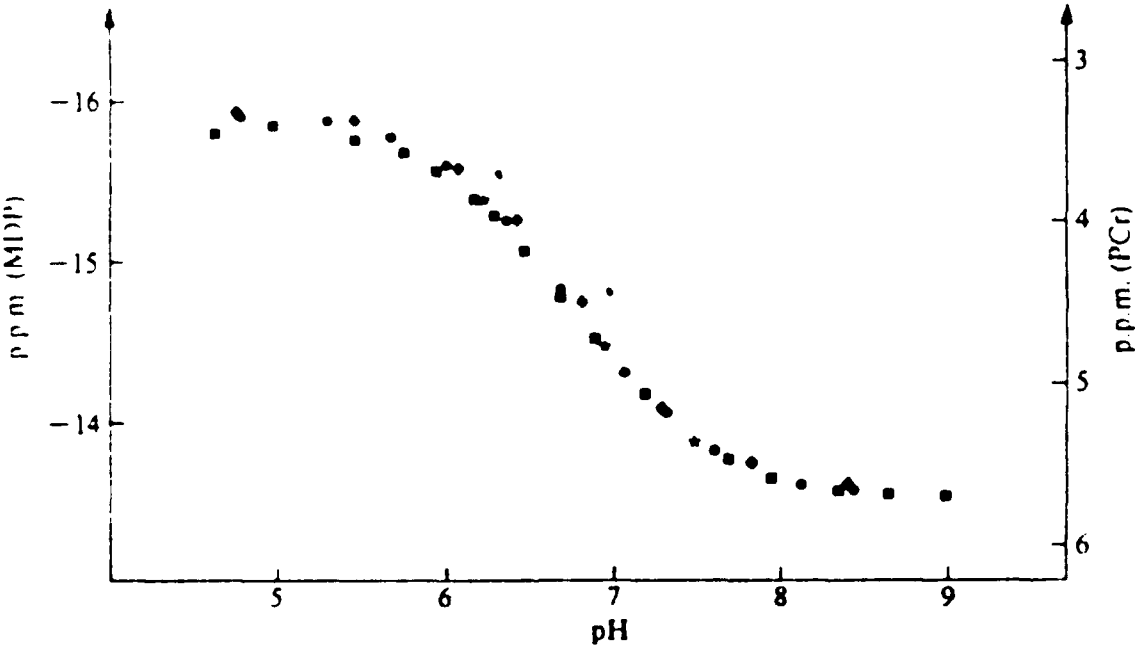

Chemical Shift of Pi from the Indicated Standards (MDP and PCr)

E. In Vivo 31-P NMR Spectroscopy

31-P NMR provides a non-invasive technique capable of determining the concentrations of important phosphates in living tissue. This allows the non-invasive monitoring of cellular bioenergetics and tissue pH.

Early biological NMR studies were performed on samples which could be placed in a traditional NMR tube (e.g., yeast, ascites tumor cells, or perfused organs).

The development of the surface coil rf antenna by Ackerman, et al.(5) made possible the observation of in vivo tissue resonances in whole animals. If a surface coil is placed adjacent to a sample, it will transmit and detect signals from an approximately disc-shaped region of the sample immediately in front of the coil, of radius and thickness approximately equal to the radius of the coil. The advantage of the surface coil is that in the study of many biological systems (e.g., kidney) it is not necessary to surround the sample by an rf-coil but rather to stimulate signals from topical application. However, the major disadvantage of the surface coil is that the magnetic field generated within the sample is not uniform. When sample geometry allows, a solenoidal rf coil surrounding the sample is preferable. The magnetic field over the sample volume is then much more uniform, leading to increased signal-to-noise ratio and sampling more representative of the average. For protruding subcutaneous

tumors the solenoidal coil is generally chosen.

In vivo 31-P NMR has enabled investigation of animal models for normal and patho-physiology, as well as clinical studies in man.

1. Heart. The first use of NMR to study tissue involved excised muscle (6). This lead directly to an investigation of the feasibility of NMR for measurement of phosphate metabolism in perfused hearts. It was quickly demonstrated that anoxia or ischemia results in rapid depletion of the high energy compound, PCr, accompanied by a rise in Pi and a downfield shift of the Pi peak indicative of tissue acidosis. Figure 5(a) illustrates the 31-P spectrum of a well perfused heart, with Figure 5(b) showing the changes associated with induced ischemia (6).

2. Brain. NMR has also been used as an investigative tool for the metabolism of brain tissue. Chance and coworkers were the first to obtain 31-P NMR spectra from the head of an anesthetized mouse. Ischemia in brain tissue produces the same changes as observed with heart tissue ischemia. Further areas of investigation have been reperfusion following ischemia, seizures, hypoglycemia, anoxia, anesthetics, metabolic inhibitors and ischemic birth insult in humans (for a review see reference 7). Brain tumors also appear to be a promising area for application of NMR, as the phosphorus metabolites of most

Figure 5

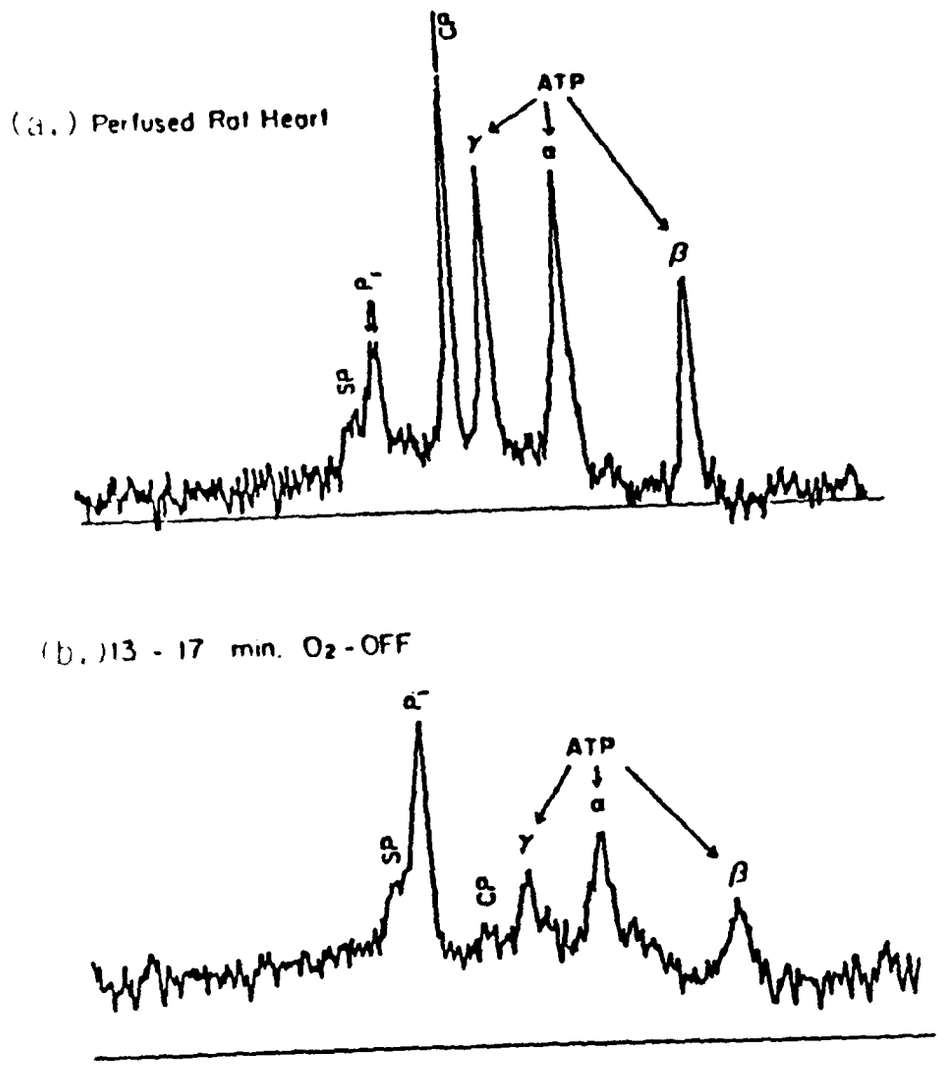

Perfused vs Ischemic Rat Heart

tumors are quantitatively different from those of normal brain.

F. 31-P NMR in Malignancy

Figure 6 displays a typical in vivo spectrum obtained at 8.5 Tesla of a Radiation Induced Fibrosarcoma (RIF-1) tumor growing on the flank of a C3H/HeN mouse.

Considerable variability has been observed in the metabolic characteristics of tumors as monitored by NMR spectroscopy, even for the same tumor line at the same stage of tumor growth (8). This illustrates the ability of NMR to monitor metabolic differences among apparently similar tumors. The differences observed between 31-P NMR spectra of different tumor lines are primarily in the relative concentrations of the detected phosphate metabolites, rather than the appearance of new resonances. The same can be said when comparing tumor spectra to spectra of normal tissue. However some tumors appear to lack PCr entirely and this has been related to certain types of drug-resistance (9).

Unlike other normal adult tissues, profound changes are observed in the 31-P NMR spectra of murine tumors during untreated growth (3, 10).

Figure 7 displays the 31-P NMR spectra of a representative RIF-1 tumor at different stages of growth after subcutaneous implantation on the flank of a C3H/HeN mouse.

The initial spectrum contains intense NTP and PCr resonances but already indicates a slightly acidic pH. As

Figure 6

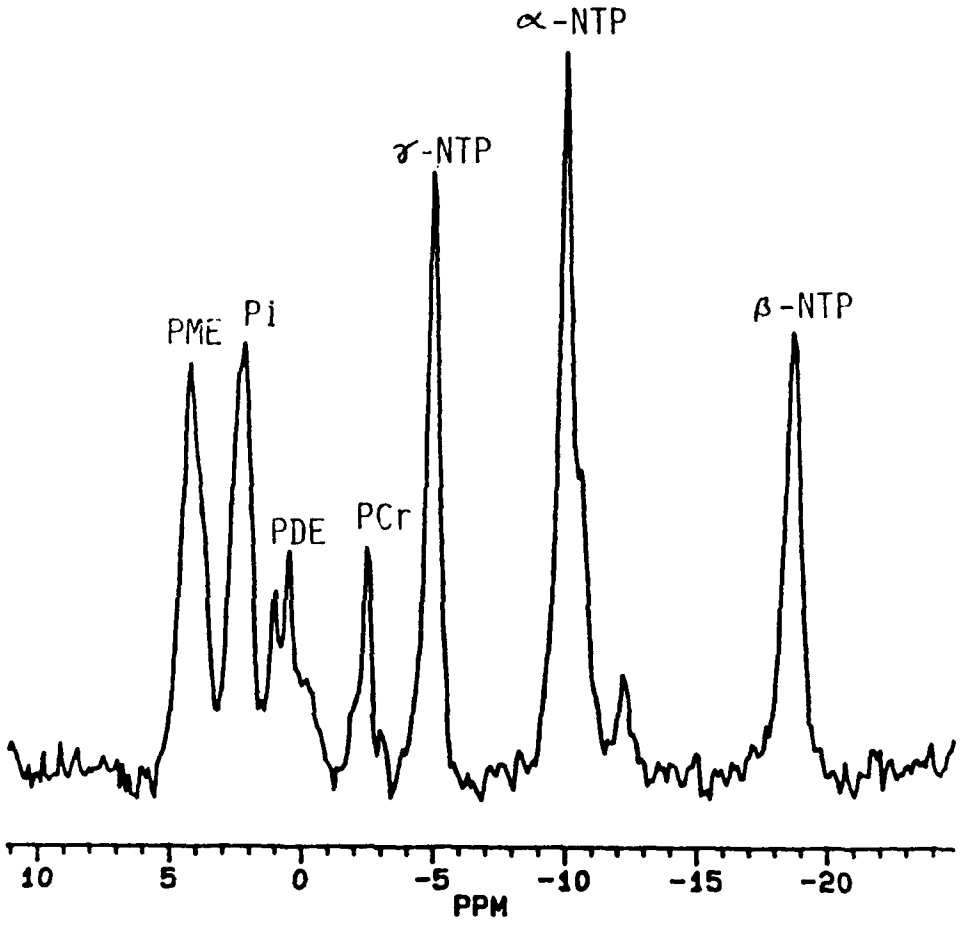

In Vivo 31-P NMR Spectra of RIF-1 (8.5T)

Figure 7

CONTROL

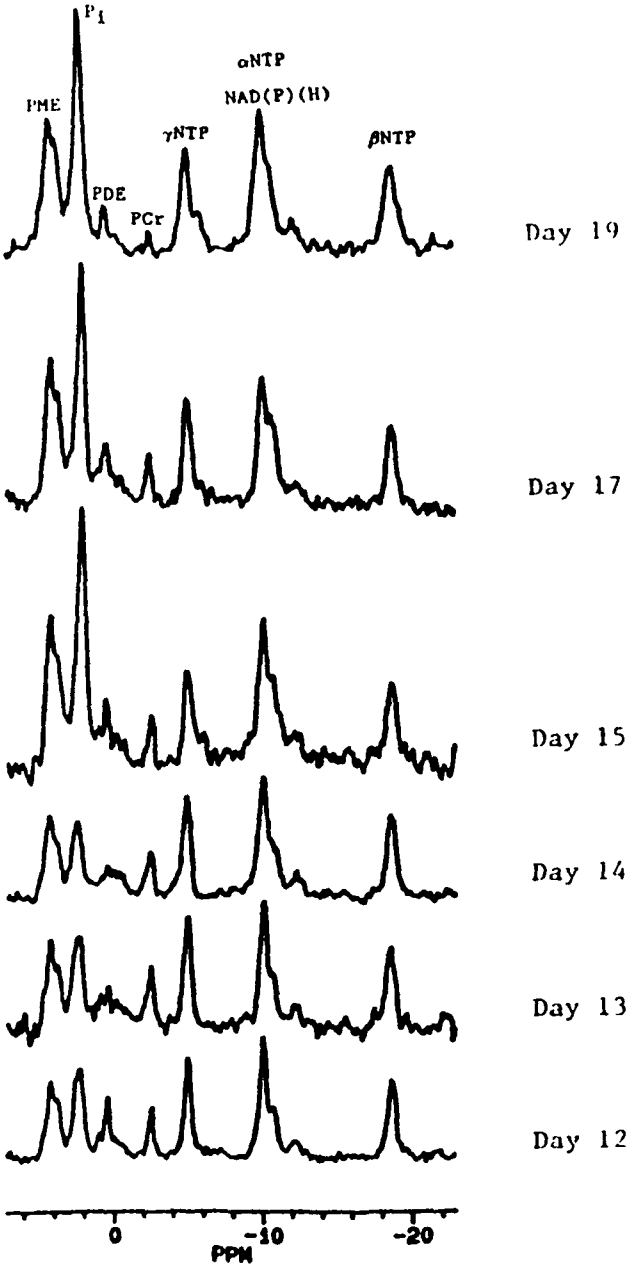

Untreated Growth of RIF-1 Fibrosarcoma

the tumor mass grows, a significant upfield shift (indicative of acidosis) and an increase in Pi occurs, with a concomitant decrease in PCr. The NTP peaks are not significantly altered. These spectral changes are similar to those exhibited by a number of other tumor lines (3,11). In contrast, some tumor lines such as the MOPC 104E myeloma and the rat 9L gliosarcoma (12) have similar levels of high energy phosphates (i.e., NTP and PCr) in the early stages of growth, but show a much more rapid and extensive decline in the later stages of growth, with the PCr and NTP peaks falling below detectable levels in 31-P NMR.

Because spectra of advanced tumors often resemble ischemic normal tissue, the spectral changes during untreated tumor growth have been attributed to the progressive development of tumor vascular insufficiency. A potential model for the interpretation of this phenomenon includes three general subpopulations of tumor cells, whose proportions vary with the stage of tumor growth (13). The first subpopulation is described as aerobic cells, metabolically active and proliferating, located in relatively close proximity to functional blood vessels. These cells obtain energy by a combination of oxidative phosphorylation and aerobic glycolysis, with the proportion determined by the genetic predisposition of the particular tumor line. The second subpopulation consists of hypoxic cells which are more remote from functional blood vessels: some of

these cells have sufficient glucose to sustain a relatively high level of anaerobic glycolysis, while others are bioenergetically inert and tend not to proliferate. The final subpopulation consists of necrotic cells that have died and are in various states of decomposition. In early stages of growth, aerobic cells predominate in the well-vascularized tumors, while in later stages of growth, hypoxic cells predominate and the tumor mass exhibits a gradual transition to a more metabolically inactive state. In still later stages, more cells are metabolically inactive (hypoxic) or necrotic. The observed spectrum is due to a superposition of the spectral characteristics of these cellular subpopulations.

Recently it has been proposed that the environmental heterogeneity in the tumors results not only from the proximity to blood vessels, but also from fluctuations in flow through these vessels in the tumor (14). Evelhoch, et al (8) found that for the RIF-1 tumor, pH, PCr/NTP and Pi/NTP were not well correlated with tumor mass, but were highly correlated with the size of the well-perfused fraction of the tumor, as measured by an 15-Oxygen washout technique. In the FSaII fibrosarcoma, which shares similar spectral properties with RIF-1, Okunieff et al (15) report that the progressive decrease in high energy phosphates (i.e., NTP and PCr) and increase in low energy phosphates (i.e., Pi) observed as tumors grew, paralleled an increase

in the radiobiological hypoxic fraction, as measured by the paired survival assay technique.

G. 31-P NMR Spectroscopy of Humans

With the introduction of large bore magnets at relatively high fields (1.5 - 2.0 Tesla) and the development of methods for spatial localization, it has been possible to initiate studies of tumors in human patients using 31-P NMR spectroscopy. For tumors near the surface of the body, surface coils similar to those used for animal studies have been frequently used, because of their ease of implementation and high sensitivity. However, studies of more deep-seated tumors, especially in the brain, are now possible. Two major categories of localization methodology are currently in use. The first uses the magnetic gradients of the NMR imager to selectively excite and/or receive signals from a known volume within the body ("Bo methods"). The second uses the non-homogeneity of the radiofrequency signal of the surface coil to isolate a region from which coherent signal is obtained ("B1 methods").

Reports of studies of human tumors using NMR spectroscopy are still largely anecdotal. Maris, et al. (16) reported two cases of pediatric neuroblastoma in the liver. The major difference between tumor and normal liver was a highly elevated phosphomonoester (PME) resonance in the tumor, which was reduced to the level of normal liver as the tumor responded to chemotherapy. High resolution extracts of the resected tumor revealed that the PME resonances resulted from the phospholipid precursors

phosphocholine (PC) and phosphoethanolamine (PE), compounds which are also found to be elevated in neonatal brain, relative to adult brain (17). The authors proposed that this characteristic may be related to rapid cell growth, in the neonatal or malignant condition. Elevated phosphocholine has also been identified in human lung cancer, and is absent from healthy adult lung (18). A survey of 15 human tumors at various sites examined in vivo by Oberhaensli, et al. (19) revealed a striking diversity of 31-P NMR spectra. In the entire group Pi levels were slightly to greatly elevated. The brain tumors examined all had lower PCr/ATP than normal brain, and 6 of 8 had higher levels of PME. The two liver tumors had higher PME than normal liver. The primary hepatoblastoma lacked PCr, as does normal liver, but a secondary endometrial adenocarcinoma in the liver had a high PCr level, making it easily detectable. Treatment of this metastasis by embolization to induce tumor ischemia resulted in a dramatic reduction in PCr and tumor pH, with an elevation in Pi, changes similar to those observed in heart and brain during ischemia.

H. Response of 31-P NMR to Radiation Therapy

Glickson and Griffiths were the first to report that 31-P NMR spectra from experimental tumors showed rapid changes after initiation of a wide variety of therapies (i.e., anti-tumor drugs, hyperthermia, or radiation). Treatment of a subcutaneous RIF-1 tumor with radiation produces 31-P NMR spectral changes similar to those induced by the anti-tumor drugs cyclophosphamide (20) and 5-fluorouracil (21). Rajan, et al.(22), observed an increase in the ratio of PCr/Pi and tumor pH with a decrease in Pi/B-NTP during days 2 through 7 following treatment with 5-20 Gray (Gy) of gamma radiation.

The pattern of 31-P NMR changes in individual tumors following radiation treatment (Figure 8) was opposite of the pattern seen during untreated growth (Figure 7). The magnitude and duration of the changes increased with increasing radiation dose. The value of the resonance ratio Pi/B-NTP on day 5 after treatment was shown by Rajan to vary linearly with the logarithm of clonogenic cell survival in the range 0-25 Gy.

Others who have investigated 31-P NMR changes associated with radiation therapy are:

1. Koutcher, et al.(23), showed that in the C3H fibrosarcoma, FSaII, small tumors (< 250 mm^3) have a greater PCr/Pi ratio and a lower hypoxic cell fraction than large tumors (> 250 mm^3). Smaller tumors, treated with

Figure 8

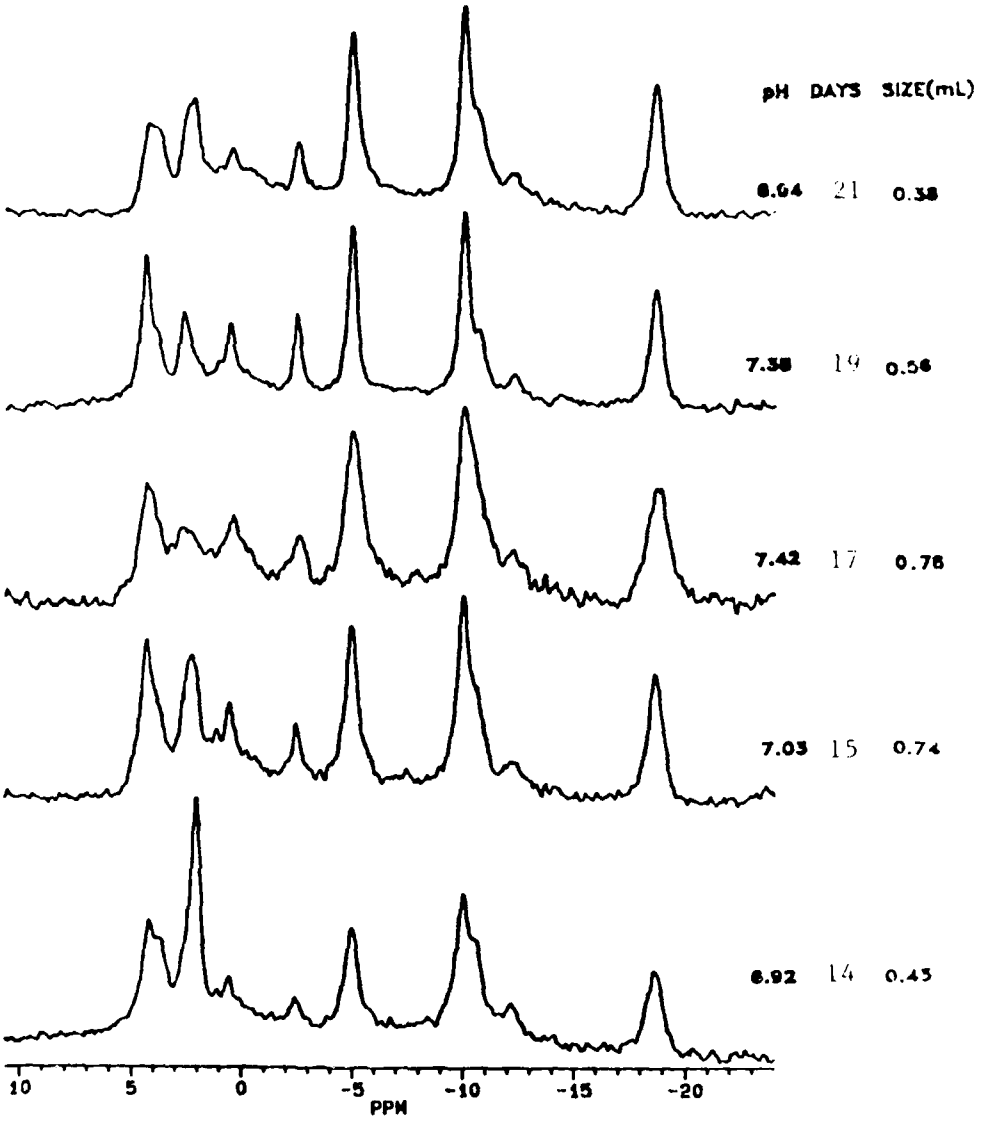

Response of RIF-1 to Radiation (14 Gy)

radiation doses chosen to induce local control in greater than 50% of animals, (e.g., single fraction between 70 and 100 Gy) showed minimal NMR changes when monitored for eight days post therapy. Tumor regression occurred by 36 hours post radiation. In contrast, large tumors showed a significant increase in the PCr/Pi ratio at 44 hours with a growth delay of 4 to 7 days following a single (70 to 100) Gy fraction. Their conclusion was that since small tumors have a minimal hypoxic fraction (= 4%), reoxygenation after irradiation would not be expected to have a large effect on the average cellular metabolism. However, large tumors of this line having a high hypoxic cell fraction (= 40%) would be expected to have a significant average change in tumor cell metabolism with reoxygenation.

2. The response of a subcutaneously implanted murine mammary carcinoma, NU-82, to 10 and 20 Gy of gamma radiation followed by in vivo 31-P NMR was reported by Sijens, et al.(24). In both the treated and untreated tumor, the necrotic fraction was found to correlate linearly with the ATP/Pi ratio. During the first 8 hours after 10 Gy the ratio of ATP/Pi increased from the control value, followed by a decrease at 47 hours. Treatment with 20 Gy caused ATP/Pi to decrease gradually through 48 hours. During the observation period of 48 hours, no change in size or pH was observed at either radiation dose. However, the PDE resonance did decrease in intensity.

3. Similar studies were performed in the RIF-1 tumor by Bhujwalla, et al.(25). Their results showed no significant correlation between the necrotic fraction and any NMR parameter after 20 Gy of radiation. Also, following irradiation the ratios of PCr/Pi, ATP/Pi, and pH showed significant increases, as did the necrotic volume fraction.

III. MATERIALS AND METHODS

A. Tumor Line

The murine tumor line chosen by the NMR Research Group at Johns Hopkins University is the Radiation Induced Fibrosarcoma (RIF-1) first described by Twentyman, et al.(26). Several of the factors that lead to the selection of this tumor model were:

1. Its *in vivo* NMR spectral characteristics resemble those of human tumor xenografts of breast, lung and colon cancer (27).

2. Clonogenic cell fraction for this tumor line is high (> 25%). This allows for a significant contribution to the NMR spectra (26).

3. RIF-1 is moderately responsive to radiation and its radiobiological hypoxic fraction can be varied by changing tumor size, site of implantation, and treatment with various drugs (28).

4. This tumor model is also considered non-immunogenic and does not metastasize from subcutaneous implantation sites (26).

5. Finally, another strong consideration in favor of RIF-1 is the amount of other data available from laboratories involved with its characterization. Several key points are:

a. The RIF-1 tumor in the C3H mouse contains both acutely hypoxic and chronically hypoxic cells (29).

b. The fraction of radiobiological hypoxic cells is approximately 1% (28).

c. The RIF-1 tumor begins reoxygenation soon after irradiation. Although 100% of the surviving fraction is hypoxic after 15 Gy, within one hour the hypoxic fraction begins to fall (28).

d. The proportion of hypoxic cells following irradiation never returns to pretreatment value (10% versus 1%, respectively) (28). The RIF-1 fibrosarcoma was obtained from Dr. Robert Kallman's laboratory at Stanford University. It was maintained by alternating <u>in vivo</u> and <u>in vitro</u> passage according to the protocol of Twentyman, et al. (26). Tumors were induced by subcutaneous injection of 200,000 cells in the flank of 5 to 7 week old female C3H/HeN mice provided by the Harlan Sprague Dawley Breeders of Frederick, MD.

B. 31-P NMR Spectroscopy

1. Operating Parameters.

Spectra were acquired on a Bruker AM 360-Wide Bore spectrometer (8.5 Tesla/8.9 cm bore) interfaced to an Aspect 3000 computer. The mouse, anesthetized with Ketamine/Acepromazine, (40 mg/kg, 4mg/kg, respectively), was positioned in a plastic holder through which the tumor protruded. (Figure 9)

Coils were doubly tuned to 1-H and 31-P using the method of Rajan, et al.(30). Home-built probes containing two- to three-turn solenoidal radiofrequency coils were size-matched (2-3 cm diameter) to the tumors. Phosphorus spectra were recorded at 15 minutes after administration of anesthesia. The magnetic field homogeneity across the tumor was optimized by shimming the magnetic field until the water resonance line width (as measured as the full width at half the maximum intensity) was less than 0.3 ppm. All spectra were obtained from 200 scans with a sweep width of 8 KHz, a radiofrequency pulse width corresponding to a 65° flip of the magnetization, 3 second interpulse delay, 63.5 millisecond acquisition time, 20 Hz line broadening, and 1024 data points per free induction decay. A 160 micro second delay was used after the transmitter pulse before acquisition of data. This produced a flatter baseline in the spectrum.

Figure 9

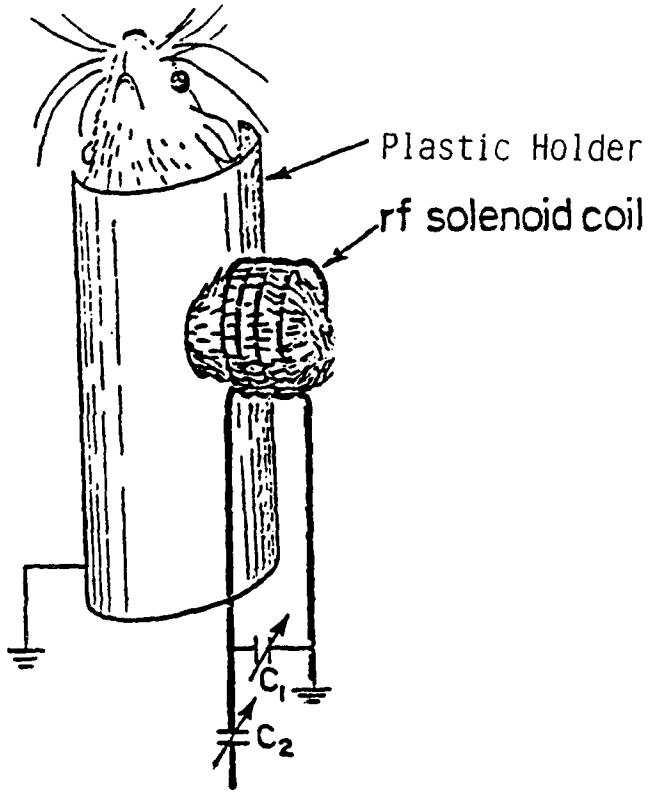

Solenoidal Coil Used for In Vivo NMR Tumor Spectroscopy in Mice

2. Spectral Peak Identification

An essential step in the interpretation of NMR spectra is the assignment of resonant frequencies to specific compounds. Figure 10(a) shows an *in vivo* 31-P spectrum (8.5T) from a subcutaneously implanted RIF-1 tumor. A corresponding spectrum of the perchloric acid (PCA) extract from the freeze clamped tumor is displayed as Figure 10(b).

31-P resonant frequencies for RIF-1 have been rigorously assigned (31) by a variety of high resolution NMR and chromatographic techniques. The nucleotide triphosphate pools of RIF-1 have been shown to contain approximately 40% non-adenine nucleotides (31). For this reason these resonance frequencies represent non-adenine triphosphate (NTP). The PME resonance originates primarily from phosphorylethanolamine (PE) and phosphorylcholine (PC). The phosphate diester (PDE) peak in the extract originates exclusively from the glycerol esters of PE and PC (GPE and GPC).

3. Peak Ratios

Integrated resonance intensities were estimated by a Lorentzian line-fitting program (GLINFIT: Bruker User Group). The free induction decay (FID) signals were subjected to exponential line broadenings (20 and 1000 Hz) prior to Fourier transformation. This served to limit the resulting spectral peaks to those peaks with line widths falling between 20 and 1000 Hz. As a result, the base line

Figure 10

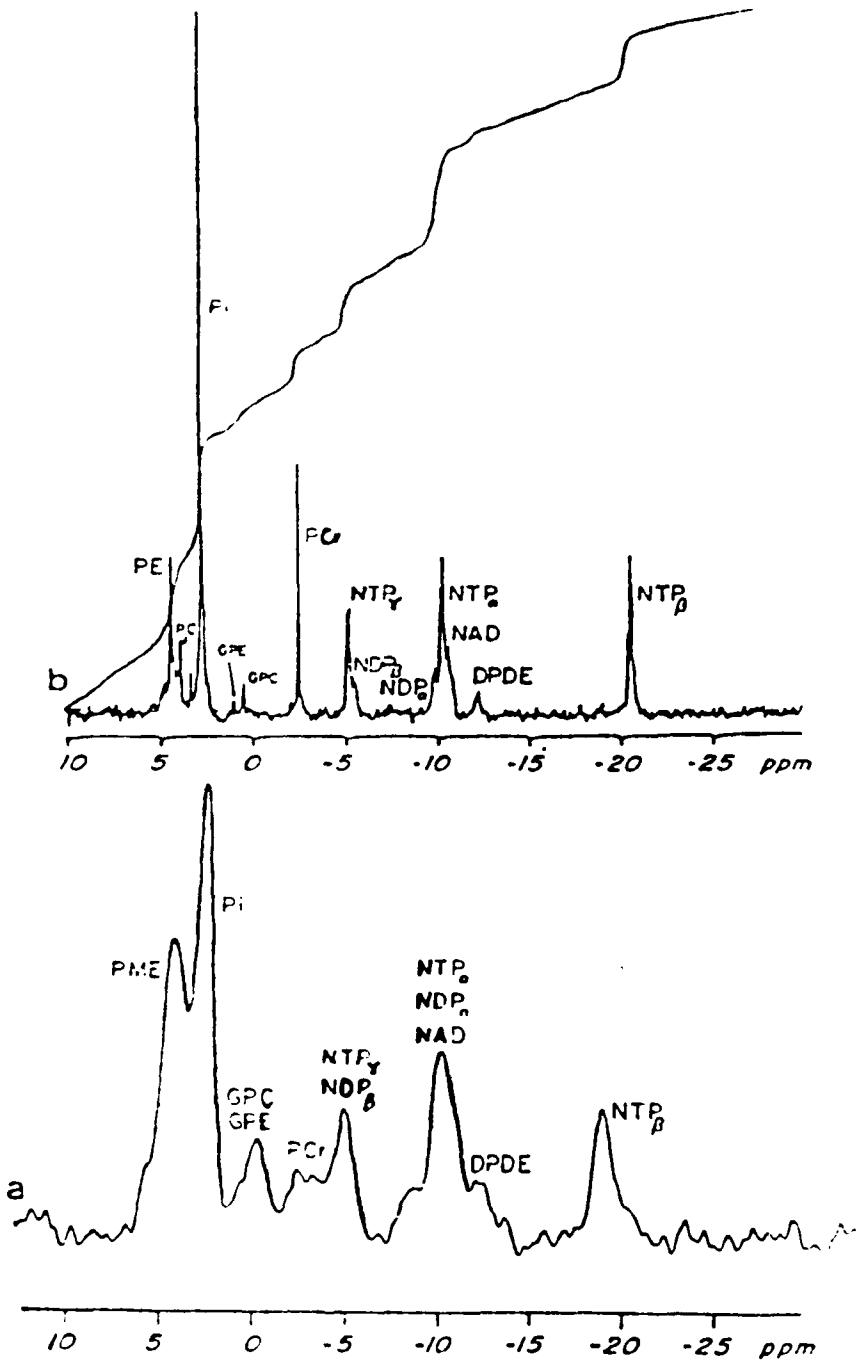

a) In Vivo 31-P NMR Spectrum

b) Perchloric Acid Extract Spectrum (from the same tumor)

is enhanced by reducing spectral noise (< 20 Hz) and eliminating the broad hump characteristic of phospholipids (> 1000 Hz).

Using in vivo rf coils it is not possible to know precisely the sampled volume or to reproduce exactly the sensitivity of signal generation and reception. For this reason absolute metabolite concentrations are not directly available at this time through in vivo spectroscopy. However, because sample volume and sensitivity are equal for all resonances in a single 31-P spectrum, ratios of metabolites can be used to compare one spectrum to another. The ratios presented here are based on integrated peak areas. In this study metabolites in the 31-P spectra have been compared to the B-NTP integrated peak area, as this resonance is well resolved in the in vivo spectrum and is present in the spectrum at all phases of growth.

4. Chemical Shift and pH Determination

31-P chemical shifts were measured using the α-resonance of NTP as an internal standard (-10.0 ppm). This corresponds to the IUPAC convention:

$$0 \text{ ppm} = 85\% \ H_3PO_4.$$

The α-resonance is present in all tissue spectra and its chemical shift is virtually pH-independent (32).

Tumor pH was calculated from the chemical shift of Pi:

$$pH = 6.803 - \log \frac{3.24 - \delta}{\delta - 0.73}$$

with δ represents the chemical shift of Pi in units of ppm (32). In those cases where two resonances of Pi were clearly discernable, they were independently integrated. For the purpose of pH analysis, a weighted average of the two chemical shifts was used.

C. Irradiation

1. Description of Irradiation Technique

A small animal irradiator, manufactured by J. L. Sheppard, with a 137-Cesium source (12,000 Curies as of November 1981), was employed for localized radiation therapy. The irradiator's collimator was employed, together with a lead brick shield to define the radiation beam. The mouse, anesthetized with Ketamine/Acepromazine in exactly the same manner as for the NMR, was placed in a plastic holder which permitted the tumor to protrude (similar to the holder shown in Figure 9.) The holder with the mouse inside was placed horizontally behind the notched lead brick body shield, which permitted the tumor to protrude into the collimated beam of gamma radiation as shown in Figure 11.

Because of the short source-to-target distance, the mouse was rotated 180° halfway through the exposure time to deliver a more nearly uniform radiation dose throughout the entire tumor.

2. Determination of Radiation Output

To confirm the radiation dosimetry, a phantom of a mouse with a representative tumor volume was constructed out of a commercially available tissue substitute. The material, known as Mix D (33), is composed of paraffin wax, polyethylene, magnesium oxide, and titanium oxide. The radiation characteristics of this substitute (compared to

Figure 11

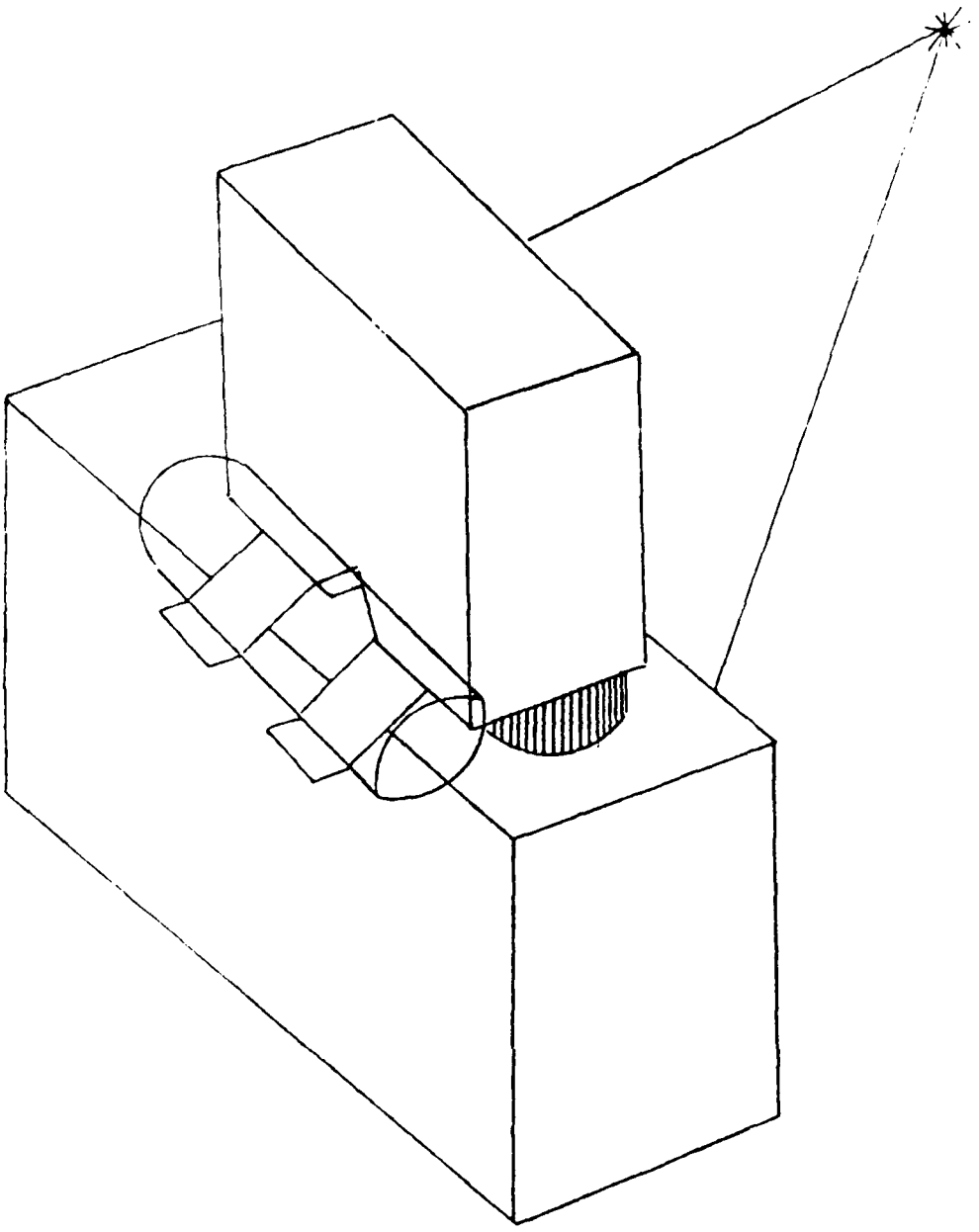

Drawing of Animal Holder Used for Irradiations

living tissue) vary by only three percent with respect to mass attenuation and energy absorption coefficients at the 137-Cs energy of 662 KeV. Thermoluminescent dosimeters, lithium fluoride disks, were embedded at the center of the tumor phantom for determination of radiation dose. These measurements yielded a dose rate of 2.61 Gy per minute.

3. Validation of Irradiation Technique

Because the technique involved localized delivery of radiation therapy it was important to determine whether or not the tumor was receiving a uniform dose of radiation. To assess this, animals irradiated via the localized technique were compared to other anesthetized animals with size-matched tumors which were irradiated whole-body. The whole-body irradiations were performed in a uniform field irradiator manufactured by Atomic Energy of Canada LTD. The estimates of clonogenic cell surviving fraction were as follows:

Table 1

Localized Versus Whole-Body Irradiation

Treatment Groups	Surviving Fraction ($x \times 10^{-2}$) $x \pm \sigma$	Number of Animals
Localized	1.37 ± 0.49	20
Whole-Body	1.46 ± 0.74	6

This difference between the two treatment groups is not statistically significant ($p > 0.5$); as determined by Student's t-test.

D. Growth Delay Studies

1. Description of Technique

When tumors had grown to a specified size (approximately 2200 mm^3 at day 14 post inoculation), they were treated according to the protocol of the particular experiment. Measurement of the tumor size was then made on a daily basis. Tumor dimensions were measured with calipers. Two perpendicular diameters (length = a and width = b) were recorded and tumor volume was calculated from the volume equation for an oblate ellipsoid:

$$\text{Volume} = (\pi/6)ab^2$$

2. Measuring Treatment Effectiveness

The values used for analysis were the Relative Tumor Sizes (RTS), the ratio of actual tumor volume to the tumor volume on the day treatment commenced. RTS provided a convenient way to standardize the data throughout the sample of tumors and involved only a negligible loss of information. Comparisons on a day-by-day basis were both cumbersome and beset by problems due to large daily fluctuations of both growth and measurement technique. Therefore as a measure of treatment efficacy, the area under the curve of RTS vs time post treatment was used (34). (Figure 12 displays how this was calculated.) The interval chosen for determination of area was the time from initiation of treatment until that point in time when logarithmic tumor growth was restored in the majority of

Figure 12

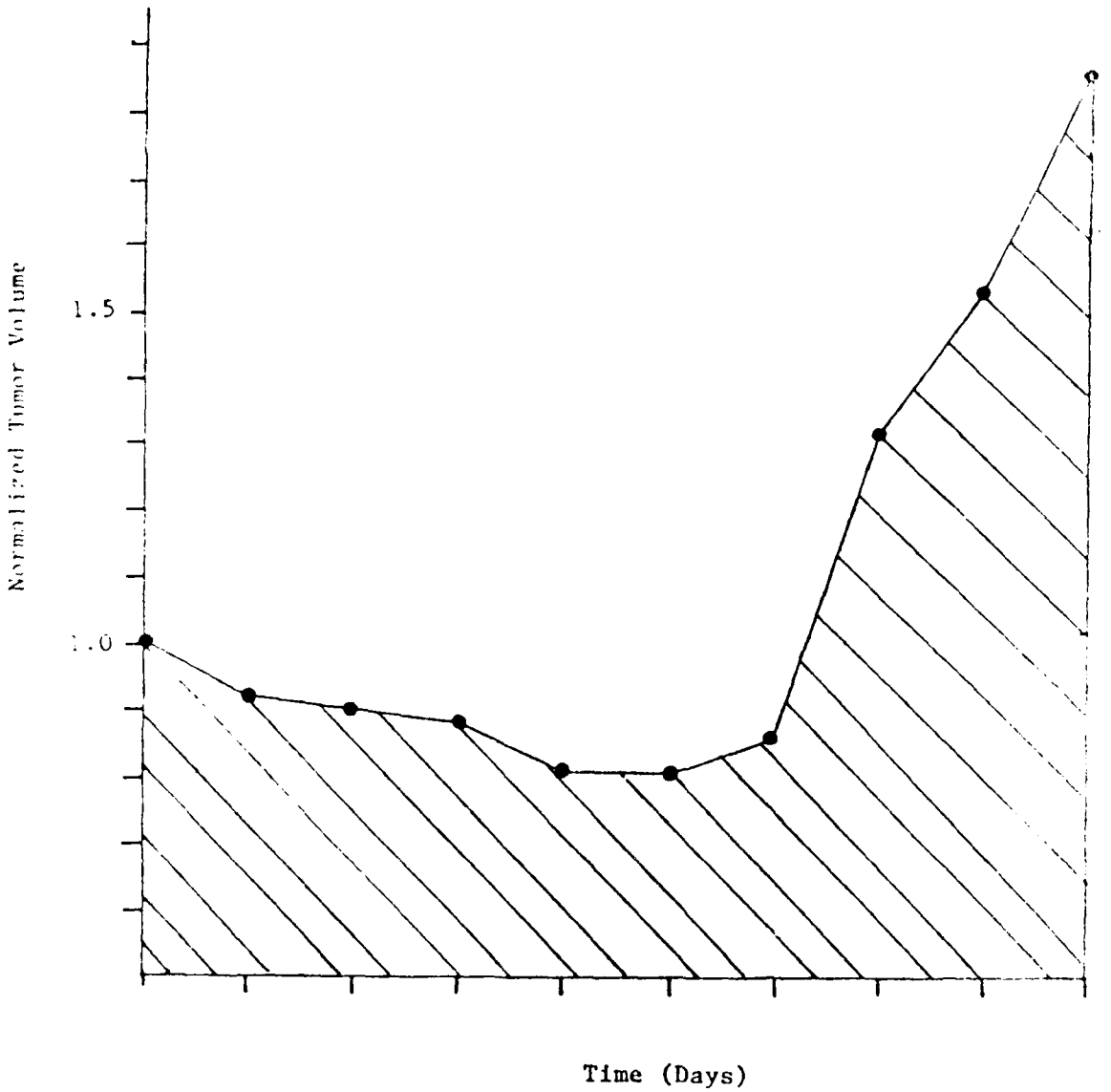

Graph Illustrating Tumor Growth After Irradiation

(Shaded area indicates the region used for the determination of Area Relative Tumor Size.)

animals treated. Smaller areas correspond to more effective treatment and larger areas indicate less effective therapy. Such a measure matches well with the visual character of the graph and accounts for both degree and duration of inhibition. In addition, daily fluctuations in volume were averaged in the process of area determination.

E. Clonogenic Assay.

1. Description of technique

The second technique used to evaluate the efficacy of radiation therapy was the *in vitro* clonogenic cell survival assay. The steps involved in this method are illustrated by the following figure. (Figure 13)

The clonogenic cell survival assay for RIF-1 was developed by Twentyman, et al. (26). It has been shown that clonogenic cell survival fraction in RIF-1 is identical when measured immediately or up to 24 hours after irradiation (35). This is consistent with the fact that *in vivo* the RIF-1 tumor lacks the potential to repair any lethal damage. Following radiation treatment, the animal was sacrificed via cervical dislocation and the tumor was removed, minced, and enzymatically digested to a suspension of single cells. The cells were counted in a hemocytometer, and known numbers of cells were plated in complete growth medium (RPMI 1640, 10% FBS, Penicillin/ Streptomycin). All plates were incubated at 37° C for a period of 10 to 14 days.

After incubation the following can be observed:

a. Some of the seeded cells are still single and have not divided.

b. Some cells have managed to complete one or two divisions to form a tiny abortive colony.

c. Some cells have grown into large colonies. These

Figure 13

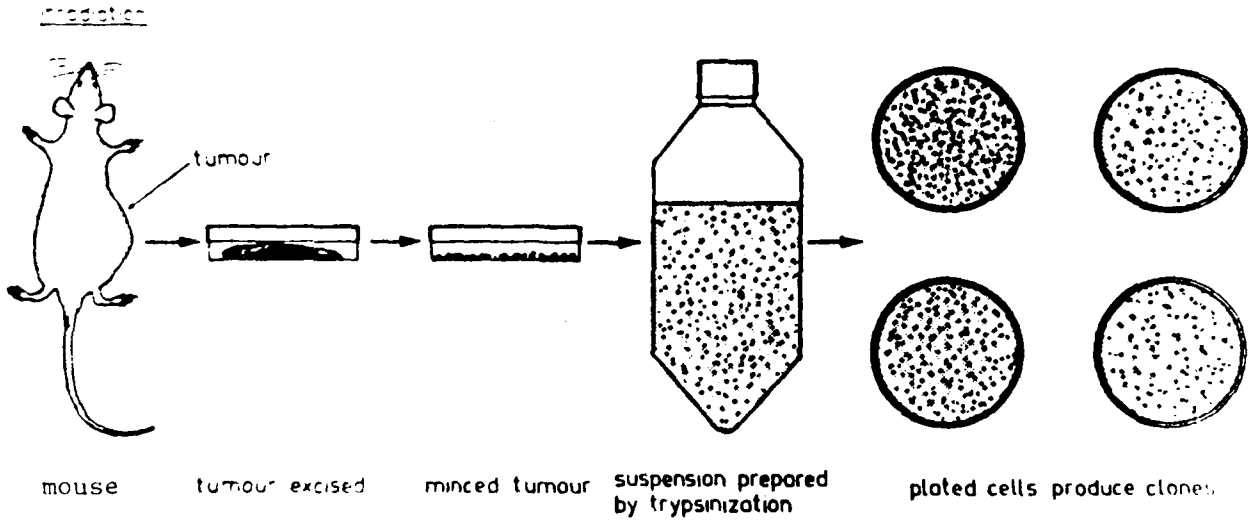

Representation of the Steps Involved in Clonogenic Cell Survival Assay

cells are said to have "survived" and are "clonogenic" in that they have retained their reproductive integrity. A colony was defined as a cluster of at least 50 cells.

2. Evaluation of Results

Treated cells were plated in triplicate at a minimum of two, but usually three dilutions. Additionally, control plates were prepared from untreated tumors. These control plates prepared from untreated tumors were used to determine the overall assay plating efficiency (PEc) by dividing the number of colonies produced by the number of cells seeded.

Individual plate estimates for surviving fraction were calculated by:

$$\text{Surviving Fraction} = \frac{\text{Colonies Counted}}{\text{Cells Seeded} \times \text{PEc}}$$

The lower the estimate of surviving fraction the greater the relative radiosensitivity. The criterion used for selecting the best estimate of surviving fraction was to choose that estimate from plates with the lowest cell concentration which also produced colonies in all treated animals.

IV. EXPERIMENTAL RATIONALE

The following hypothesis was tested: *In vivo* Phosphorus-31 NMR Spectroscopy can be used to forecast tumor response to radiation therapy.

This project had two specific aims:

a. Determine whether pre-treatment NMR spectra can predict the outcome of single fraction radiation therapy.

b. Determine if optimal timing of successive doses of radiation (i.e., fractionation) can be predicted on the basis of NMR spectral properties of the tumor at the specific time of treatment.

For the single fraction experiments, tumors were assessed by NMR spectroscopy in their natural state as well as following administration of drugs known to alter their radiosensitivity. The first step was to identify differences in NMR spectral parameters and then correlate those differences with accepted indices of radiation sensitivity.

In the fractionated therapy experiments, NMR spectral parameters were evaluated prior to the priming dose and prior to the second fraction which was shifted to various time intervals (0 to 72 hours). Relative values or changes of NMR parameters were identified and correlated with the ultimate outcome of fractionated radiation therapy.

V. RESULTS

A. Single Dose Experiments

In an attempt to determine if 31-P NMR Spectroscopy can serve as a predictor of radiation therapy efficacy, the following experiments were undertaken.

1. Tumors in Their Natural State vs Hydralazine Treated

a. Tumors in Their Natural State. Since a considerable degree of variability has been noted by others in the NMR spectra of RIF-1 tumors, even at the same stage and size of tumor growth (8), twenty animals with 14 day old tumors in their natural state were first measured via in vivo 31-P NMR spectroscopy and then irradiated with a dose of 15 Gray. Within 4 hours after irradiation the animals were sacrificed and clonogenic cell survival assays performed on their tumors to assess radiation sensitivity. For each animal the values of various NMR parameters before treatment were compared with the estimate of radiation sensitivity of the tumor (i.e., surviving fraction). Although several NMR parameters were evaluated, only two parameters showed correlations with radiation sensitivity which had R values greater than 0.50. These were pH and PCr/Pi. These correlations with surviving fraction are shown in Figures 14 and 15, respectively.

The slope for each relationship was negative, which indicates that as pH or PCr/Pi increased, the radiation

Figure 14

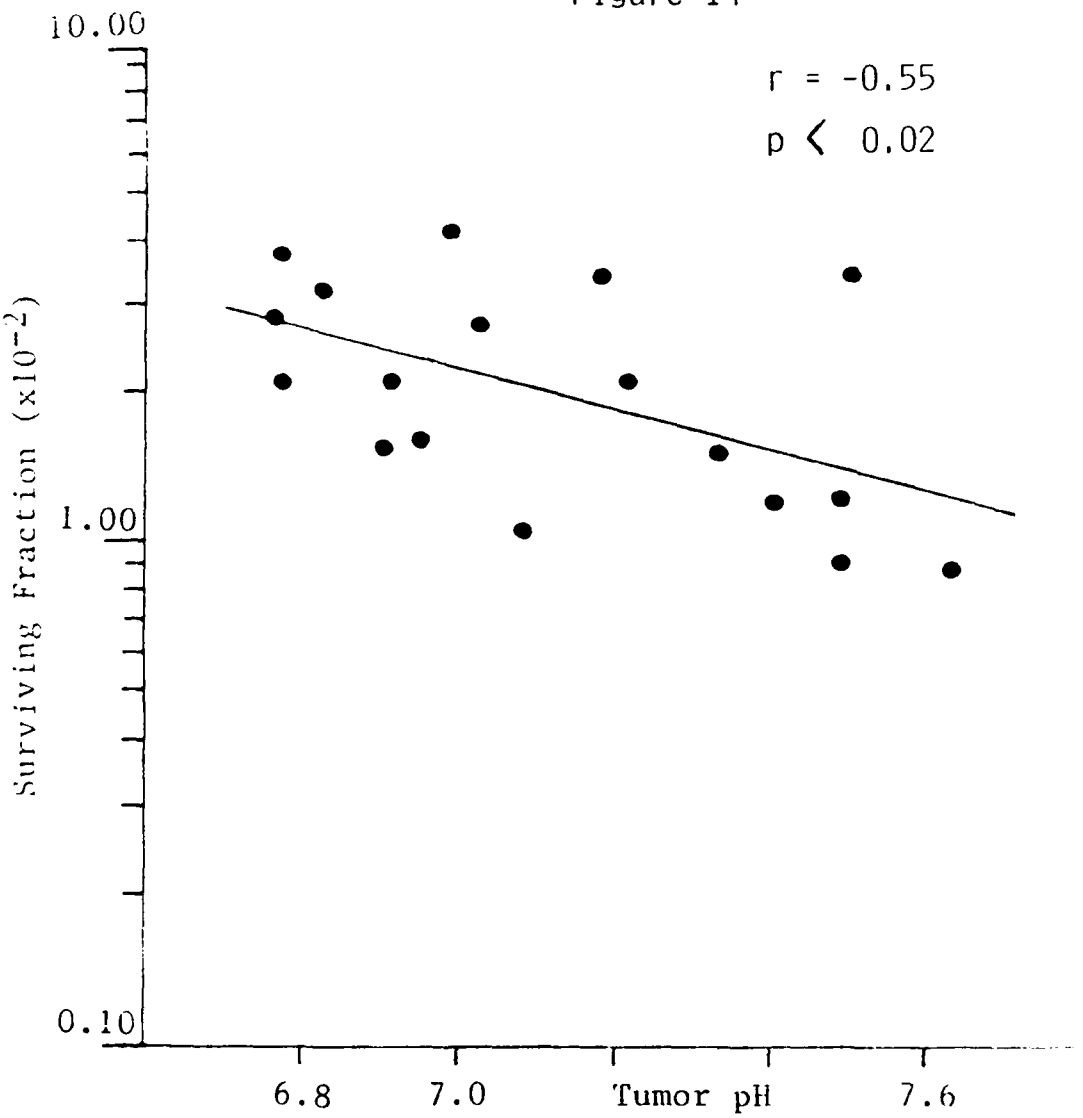

Tumors in Their Natural State
Surviving Fraction (15 Gy)
vs
Pre-Radiation Tumor pH

Figure 15

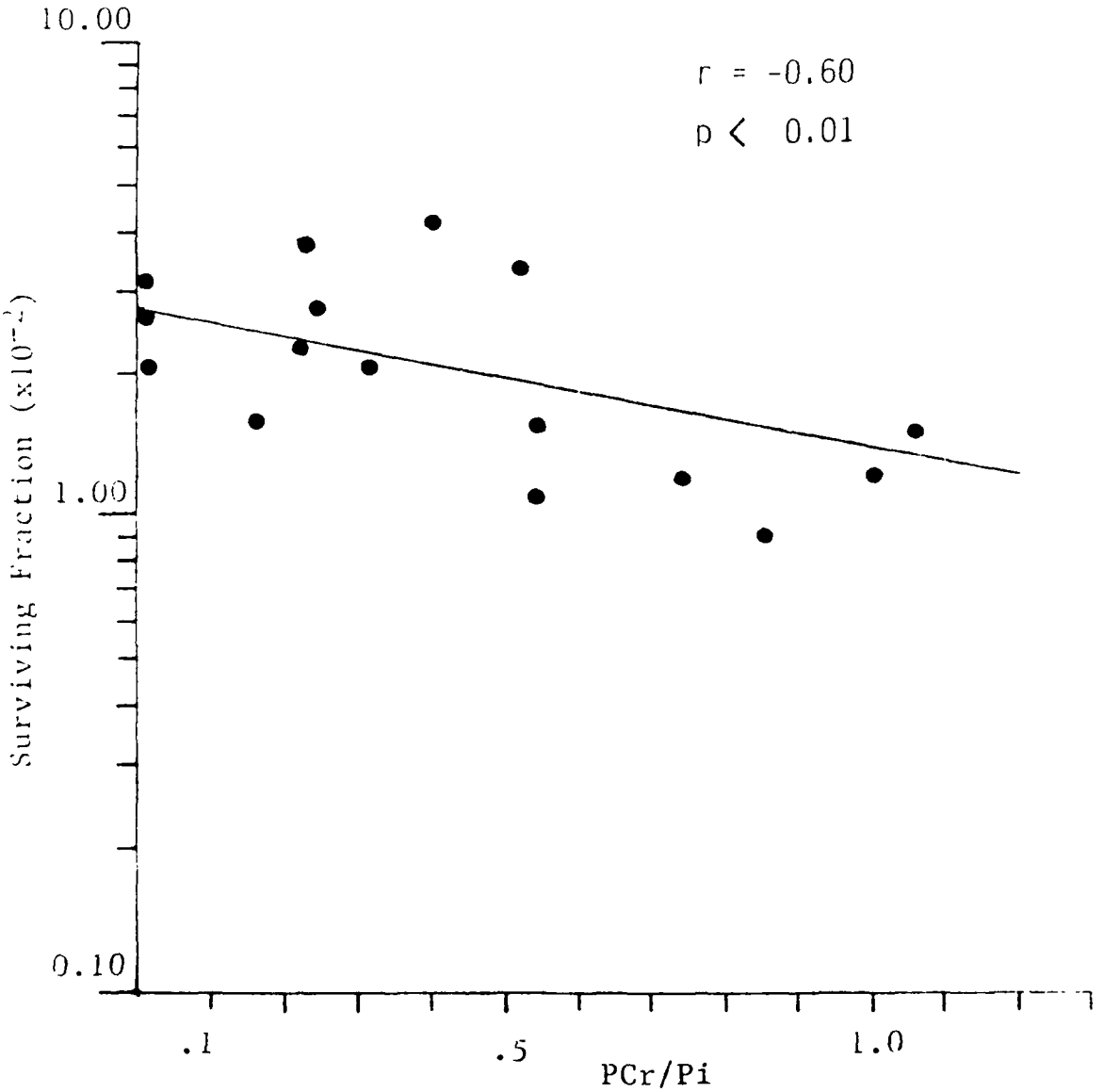

Tumors in Their Natural State

Surviving Fraction (15 Gy)

vs

Pre-Radiation Tumor Pcr/Pi

sensitivity of the tumor increased as well (i.e., surviving fraction falls).

b. Tumors Treated With Hydralazine. The drug hydralazine has been shown to reduce radiation sensitivity in tumors. The drug acts as a vasodilator on the systemic circulation, yet fails to affect the vasculature to the tumor. This increase in relative vascular resistance results in decreased tumor blood flow and decreased radiation sensitivity (36, 37).

For these experiments 14 animals were first treated with hydralazine (2.5 mg/Kg or 10 mg/Kg) and then evaluated by 31-P NMR, after which, the animals were irradiated within 2 hours with a dose of 15 Gy. Again, the animals were sacrificed and a clonogenic assay was performed within 4 hours to assess radiation sensitivity. Like the tumors evaluated in their natural state, the hydralazine-treated tumors showed a correlation between surviving fraction and pH and PCr/Pi. (Figures 16 and 17 respectively).

Here, too, the slopes of the relationships were negative, indicating that as PCr/Pi or pH rose in the tumors, radiosensitivity rose as well.

2. Hydralazine, Flunarizine and Saline Treated Tumors

a. Time Course of NMR Changes. During the course of the previous experiment, it was observed that the NMR spectra following treatment of tumors with hydralazine were not static over time. Administration of this drug showed a

Figure 16

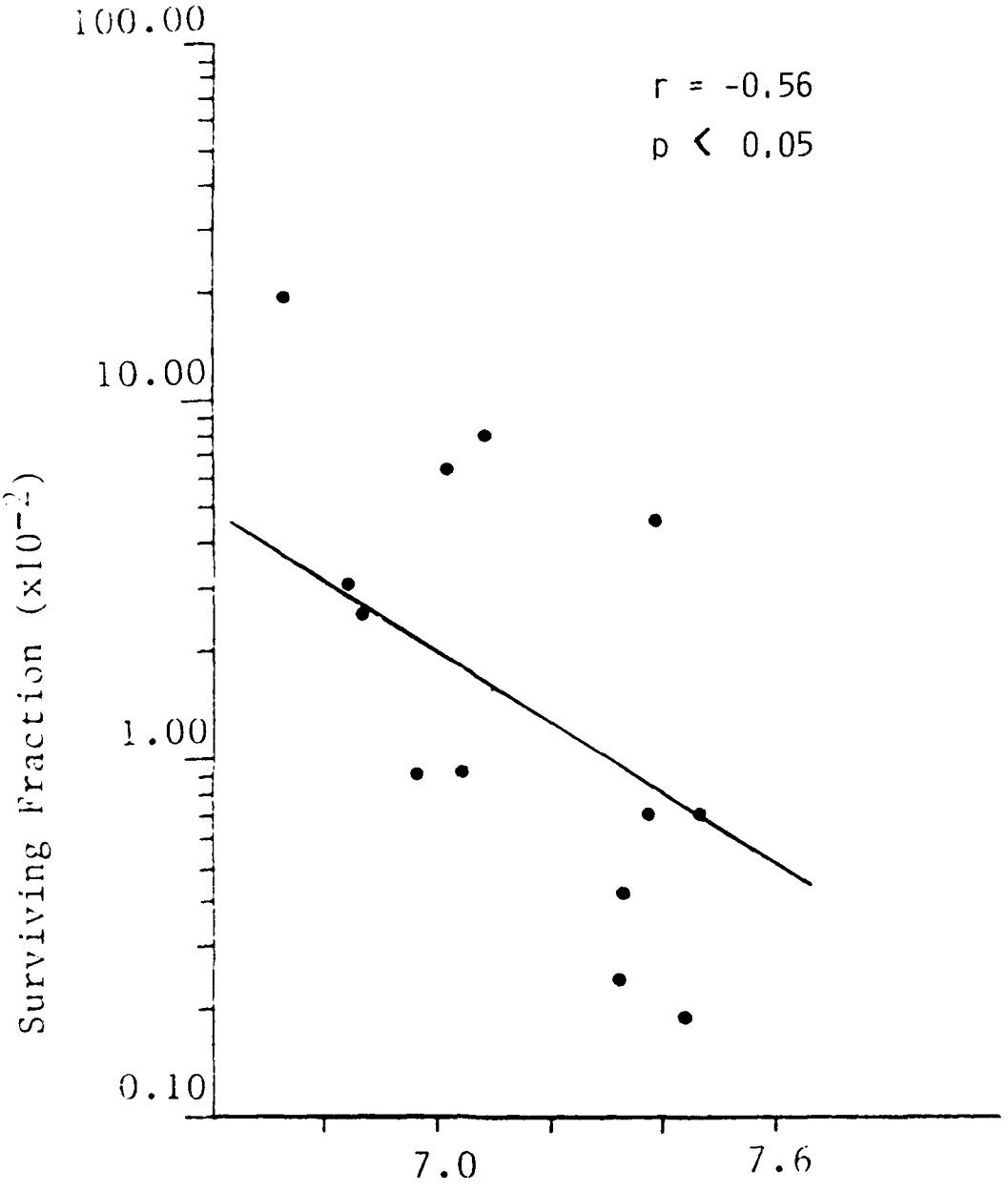

Tumors Treated with Hydralazine

Surviving Fraction (15Gy)

vs

Pre-Radiation Tumor pH

Figure 17

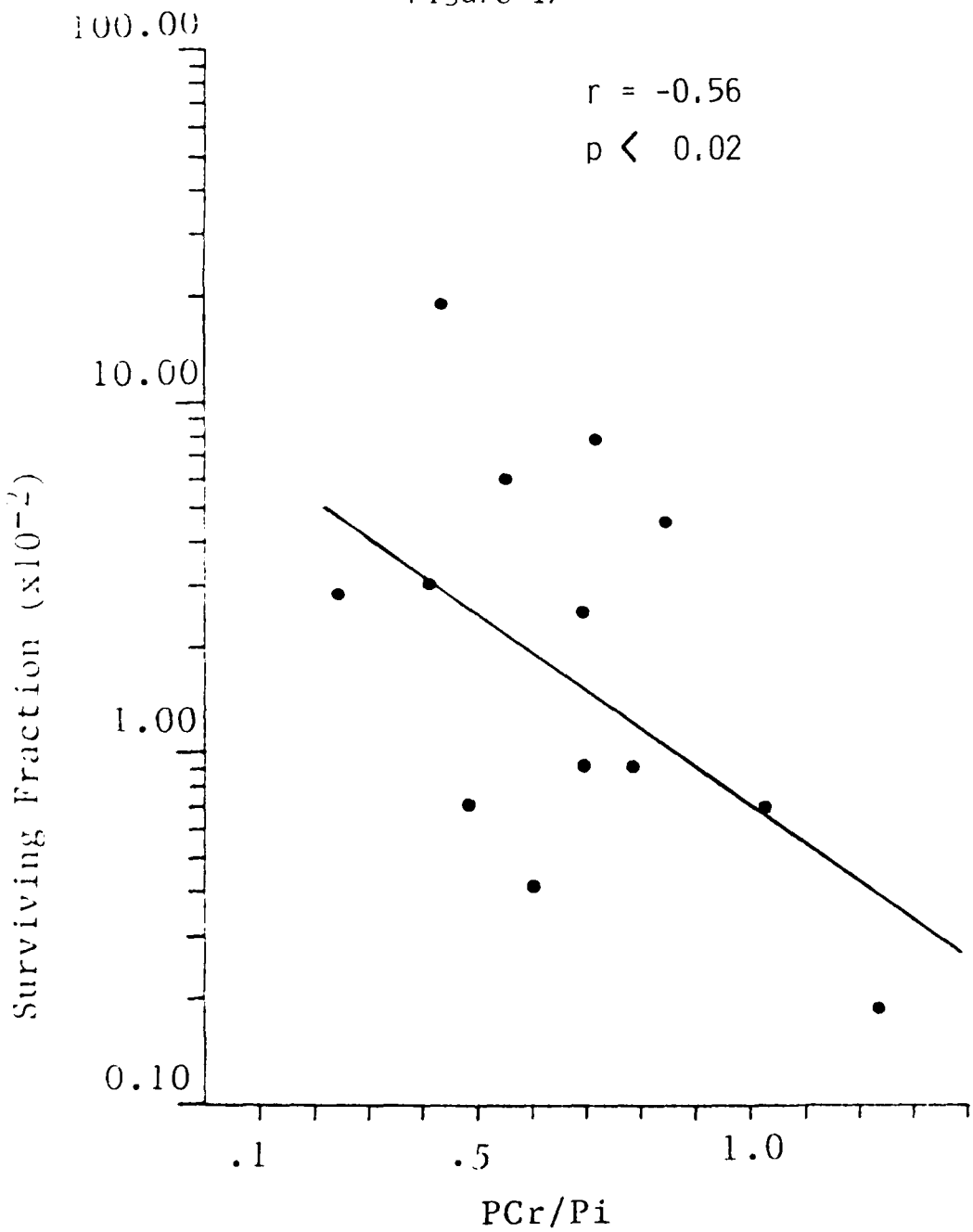

Tumors Treated with Hydralazine

Surviving Fraction (15 Gy)

vs

Pre-Radiation Tumor PCr/Pi

rapid decrease in the high energy phosphates (i.e., NTP and PCr) with an equally sharp rise in low energy phosphates (i.e., Pi) followed by a continued gradual decline in high energy phosphates. Displayed as an upfield shift in Pi, the tissue pH also declines over time (Figure 18).

In contrast to hydralazine, which leads to decreased tumor blood flow and radiation sensitivity, the drug flunarizine increases tumor blood flow and enhances radiation sensitivity (38). Time dependent changes were also observed in the NMR spectra following the administration of flunarizine (Figure 19).

In contrast to the hydralazine changes, flunarizine-treated tumors exhibit a significant decrease in low energy phosphates and a slight increase in average pH. This came not as a uniform shift in pH, but rather as a result of an increase in a clearly resolvable downfield resonance of Pi (alkaline pH).

In contrast to both hydralazine and flunarizine treated tumors, the 31-P NMR spectrum from an untreated tumor was relatively constant (Figure 20). Only a small decline in Pi/B-NTP by 60 minutes was observed, and this was probably due to the recovery of the animal from the anesthesia (4).

b. NMR Parameters Versus Radiation Sensitivity

To determine whether the differences in the NMR spectra of the hydralazine and flunarizine treated tumors

Figure 18

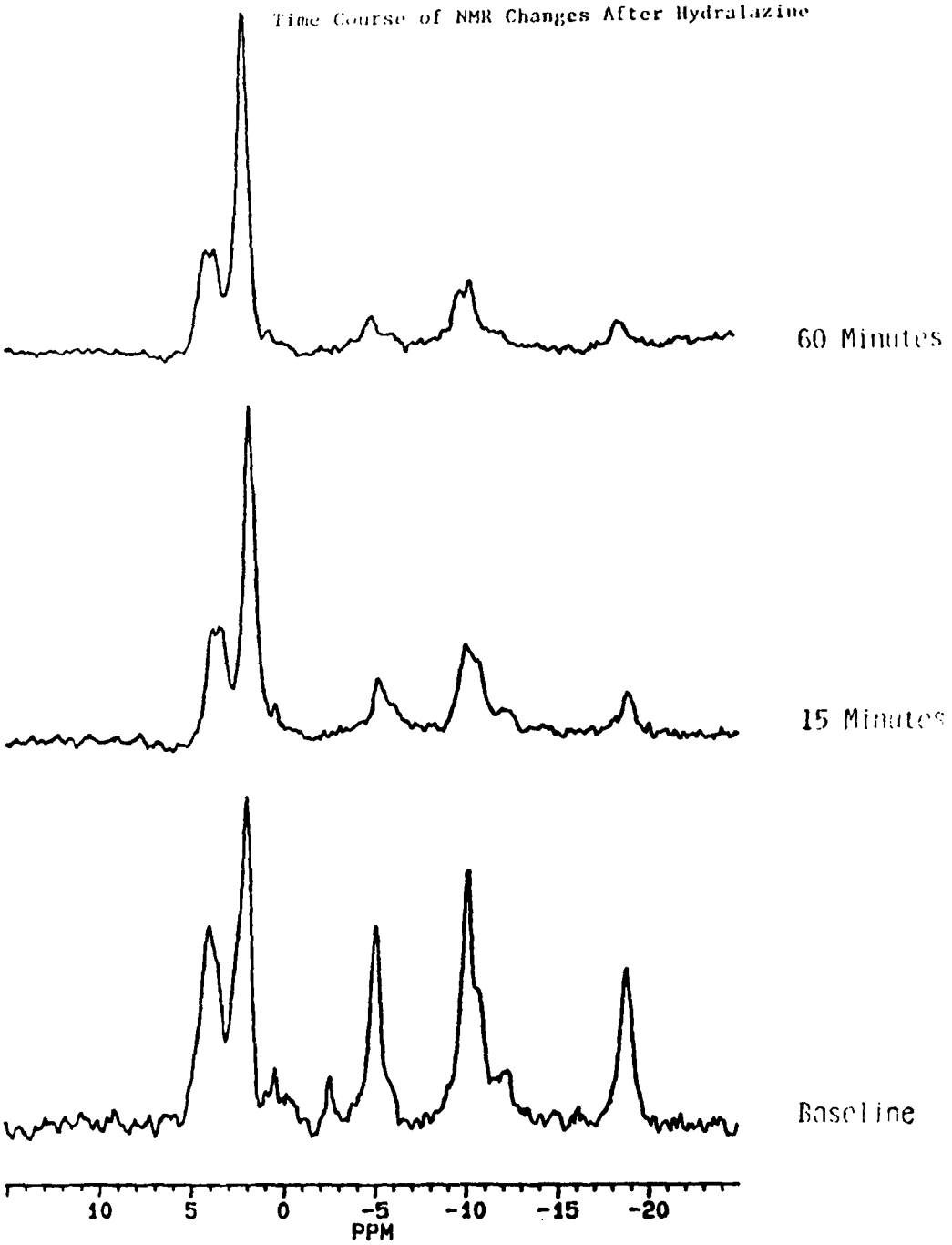
Time Course of NMR Changes After Hydralazine
60 Minutes
15 Minutes
Baseline
10
5
0
-5
-10
-15
-20
PPM

Figure 19

Time Course of NMR Changes After Flunarazine

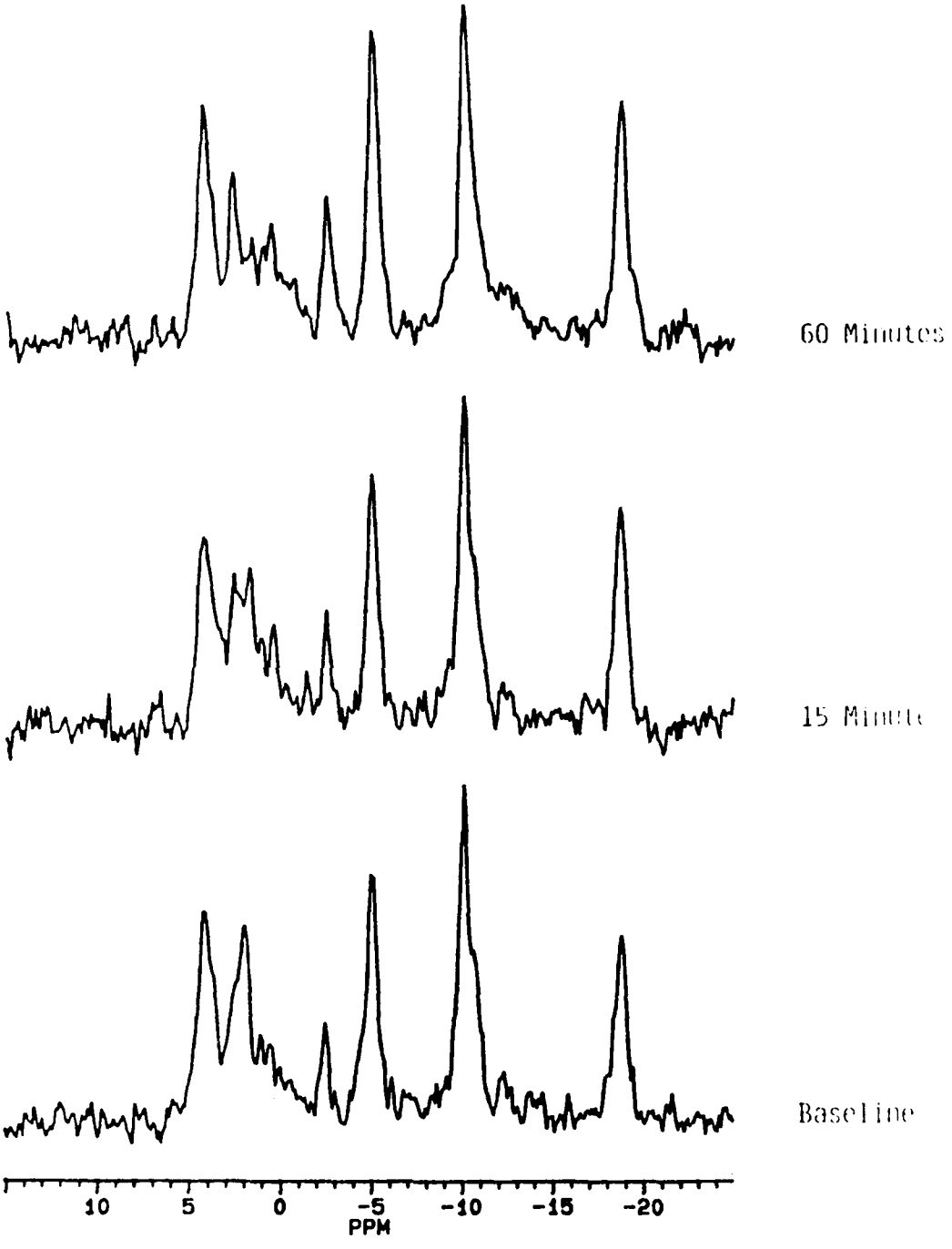

Figure 20

Time Course of NMR Spectra for Untreated RIF-1 Tumors

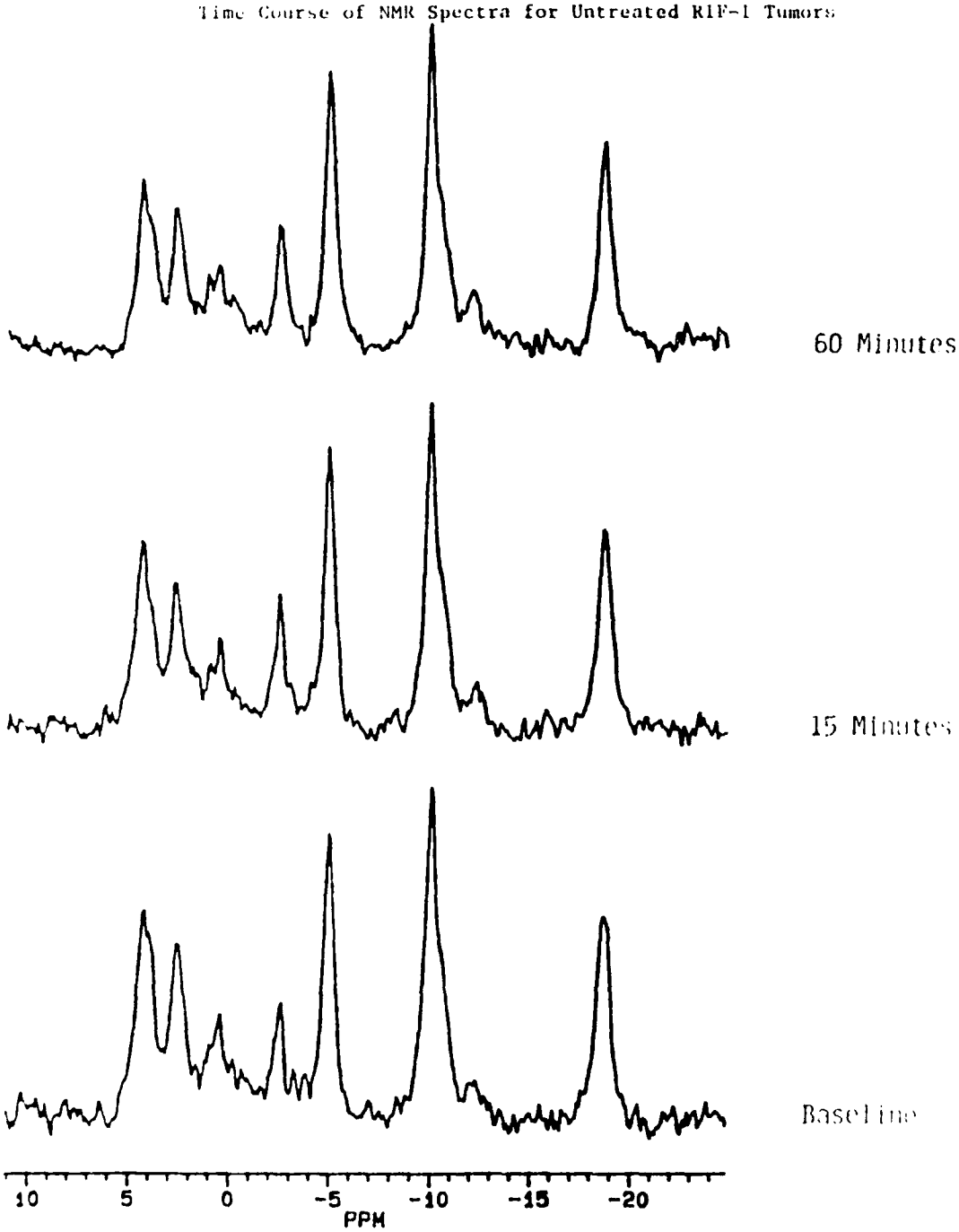

were associated with differences in tumor radiation sensitivity the following experiment was performed. A group of 18 animals each with a subcutaneously implanted tumor was evaluated by NMR to determine baseline spectra, after which each animal was treated (i.p.) with either hydralazine (10 mg/Kg), flunarizine (4 mg/Kg) or saline. Following injection of the drug NMR spectra were obtained at 15 minute intervals for one hour. NMR spectra obtained at 15 and 60 minutes post-drug treatment were used for analysis.

A second group of 25 animals was treated identically to those described above. Fifteen minutes after drug or saline treatment, the animals were irradiated with 15 Gy. These animals were then followed for a 10 day period to determine relative radiation sensitivity via tumor growth delay.

The results from the combined NMR spectroscopy (Table 2) and tumor growth delay data (Table 3) are shown in the following tables:

Table 2

Changes in NMR Parameters Following Administration of Hydralazine, Flunarizine or Saline

Treatment Group	Baseline $\bar{x} \pm \sigma$	15 Minutes $\bar{x} \pm \sigma$	60 Minutes $\bar{x} \pm \sigma$
	Tumor pH		
Hydralazine	7.12 ± 0.15	#6.76 ± 0.08	#6.65 ± 0.04
Control	7.12 ± 0.15	7.05 ± 0.30	7.09 ± 0.34
Flunarizine	7.14 ± 0.14	7.15 ± 0.12	7.26 ± 0.15
	Pi/B-NTP		
Hydralazine	1.10 ± 0.53	*3.09 ± 2.04	#4.95 ± 1.83
Control	1.25 ± 0.45	1.06 ± 0.50	*0.86 ± 0.25
Flunarizine	0.95 ± 0.26	*0.80 ± 0.23	*0.63 ± 0.16
	PCr/B-NTP		
Hydralazine	0.31 ± 0.10	*0.16 ± 0.11	#0.11 ± 0.10
Control	0.35 ± 0.11	0.42 ± 0.09	0.37 ± 0.10
Flunarizine	0.35 ± 0.02	0.36 ± 0.06	*0.42 ± 0.05
	PCr/Pi		
Hydralazine	0.34 ± 0.22	*0.07 ± 0.08	#0.03 ± 0.04
Control	0.31 ± 0.17	0.45 ± 0.17	0.49 ± 0.25
Flunarizine	0.40 ± 0.10	0.51 ± 0.24	#0.71 ± 0.24

(Matched Pairs Student's t-test between treatment time interval and baseline: * = $p < 0.05$; # = $p < 0.01$)

Table 3

Relative Radiosensitivity Following Administration of Hydralazine, Flunarizine or Saline

Treatment Group	Area RTS (thru day 10) $\bar{x} \pm \sigma$	Number of Animals
Hydralazine	13.03 ± 3.22	8
Control	11.63 ± 1.24	8
Flunarizine	10.48 ± 2.14	9

With respect to radiation sensitivity, hydralazine treated tumors were significantly different ($p < 0.05$) from the flunarizine treated tumors. However, neither flunarizine nor hydralazine was statistically different from the tumors sham treated with saline.

From the data in Tables 2 and 3, it is possible to make several generalizations. As NMR parameters PCr/B-NTP, PCr/Pi and pH increased there was an associated increase in radiation sensitivity (i.e., low RTS area). The association was reversed for Pi/B-NTP which declined with increasing radiation sensitivity.

3. Anesthesia Effects on Radiation Sensitivity and NMR Parameters.

There have been reports in the literature that sodium pentobarbital (PB) reduces tumor blood flow (39) and increases radioresistance (40). To see if these effects could be detected by 31-P NMR, a comparison was made

between PB and another anesthetic Ketamine/Acepromazine (KA). It had been noticed in hyperthermia therapy, that KA had produced a much smaller temperature drop than PB.

Twenty mice with subcutaneous RIF-1 tumors were anesthetized with sodium pentobarbital (55 mg/kg) or ketamine/acepromazine (40mg/kg and 4 mg/kg) before acquisition of *in vivo* 31-P NMR spectra. Several days later, the same animals were again anesthetized with pentobarbital (PB) or ketamine/acepromazine (KA) and then irradiated to 15 Gy. Radiation sensitivity was evaluated by growth delay. Table 4 summarizes the results from the NMR spectra.

Table 4

Changes in NMR Parameters Following Administration of Anesthetics Pentobarbital or Ketamine/Acepromazine

Treatment Group	Pi/A-NTP $\bar{x} \pm \sigma$	Pi/B-NTP $\bar{x} \pm \sigma$	PCr/Pi $\bar{x} \pm \sigma$	Pi/PME $\bar{x} \pm \sigma$
KA	*.70 ± .34	*1.11 ± .58	#.46 ± .35	*.70 ± .27
PB	1.14 ± .33	2.22 ± 1.13	.03 ± .05	1.45 ± .70

(Student's t-test: * = $p < 0.05$; # = $p < 0.01$; level of significant difference between Ketamine and Pentobarb)

PB produced a lower average ratio of tumor PCr/Pi than KA. Tumor volume regression was identical until day 5, but pentobarbitol-irradiated tumors underwent regrowth by day 7. Pre-irradiation tumor volume was achieved in day 10 in pentobarbitol-treated tumors, while ketamine-treated tumors

did not surpass starting volume even by 16 days post-irradiation. Tumor volume was significantly smaller for the ketamine-treated group at days 7, 9, 14, and 16 following irradiation (Figure 21).

Figure 21

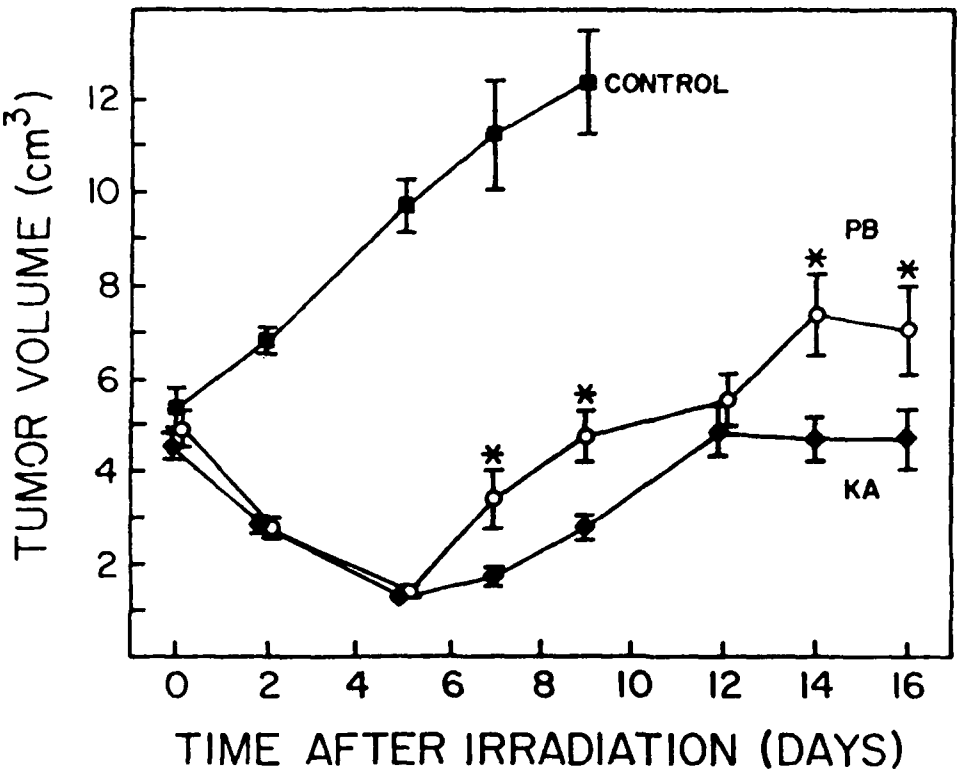

Tumor Growth Following Anesthesia and Radiation (15 Gy)

KA = Ketamine/Acepromazine PB = Pentobarbital

B. Fractionated Dose Experiments

The purpose of these experiments was to evaluate the potential of NMR spectroscopy to predict optimal timing for fractionated radiation therapy.

1. Determination of Optimal Timing

In these experiments, animals were randomly assigned to treatment groups designated as 0-0, 0-8, 0-16, 0-24, 0-48, and 0-72, referring to the time in hours at which fractionated radiation therapy (10 Gy per fraction) was delivered. For each of the animals described above, NMR spectra were obtained prior to any radiation therapy (i.e., pre-treatment spectra) and then again after the first fraction of radiation therapy but just prior to the second fraction (i.e., post-treatment). The means for values of NMR parameters and pH are compared pre-and post-treatment (10 Gy) for each of the treatment intervals in Table 5:

Table 5

NMR Parameters Measured Before Radiation Therapy (10 Gy) and Immediately Prior to Second Fraction

Treatment Group	NMR Parameter	Pre-Treatment $\bar{x} \pm \sigma$	Post-Treatment $\bar{x} \pm \sigma$
0-0	PME/B-NTP	1.06 ± 0.34	(a) N.A.
n=11	Pi/B-NTP	1.03 ± 0.60	N.A.
	PDE/B-NTP	0.62 ± 0.23	N.A.
	PCr/B-NTP	0.44 ± 0.24	N.A.
	pH	7.08 ± 0.32	N.A.
0-8	PME/B-NTP	1.33 ± 0.36	(b)*1.03 ± 0.27
n=10	Pi/B-NTP	1.74 ± 0.77	*1.17 ± 0.57
	PDE/B-NTP	0.49 ± 0.25	0.58 ± 0.25
	PCr/B-NTP	0.61 ± 0.37	0.56 ± 0.28
	pH	7.05 ± 0.16	*7.16 ± 0.15
0-16	PME/B-NTP	1.12 ± 0.33	1.15 ± 0.27
n=10	Pi/B-NTP	1.37 ± 0.67	*0.94 ± 0.32
	PDE/B-NTP	0.44 ± 0.21	0.58 ± 0.19
	PCr/B-NTP	0.66 ± 0.43	0.55 ± 0.22
	pH	7.10 ± 0.20	#7.25 ± 0.15

Table 5 (Con't)

Treatment Group	NMR Parameter	Pre-Treatment $\bar{x} \pm \sigma$	Post-Treatment $\bar{x} \pm \sigma$
0-24	PME/B-NTP	1.04 ± 0.24	1.17 ± 0.28
n=10	Pi/B-NTP	0.88 ± 0.31	0.89 ± 0.42
	PDE/B-NTP	0.52 ± 0.20	*0.81 ± 0.34
	PCr/B-NTP	0.49 ± 0.21	0.48 ± 0.16
	pH	7.22 ± 0.18	7.23 ± 0.12
0-48	PME/B-NTP	1.08 ± 0.30	1.20 ± 0.29
n=17	Pi/B-NTP	0.94 ± 0.47	0.75 ± 0.26
	PDE/B-NTP	0.62 ± 0.28	#0.78 ± 0.32
	PCr/B-NTP	0.54 ± 0.18	0.59 ± 0.18
	pH	7.13 ± 0.22	#7.30 ± 0.18
0-72	PME/B-NTP	1.24 ± 0.14	1.47 ± 0.34
n=5	Pi/B-NTP	0.96 ± 0.24	0.77 ± 0.38
	PDE/B-NTP	0.74 ± 0.13	#1.25 ± 0.14
	PCr/B-NTP	0.63 ± 0.11	0.64 ± 0.15
	pH	7.05 ± 0.22	*7.32 ± 0.18

a. N.A. = Not Applicable
b. The significance of the difference between pre- and post-treatment was determined by matched pairs t-test. (# = $p < 0.01$ and * = $p < 0.05$)

Figure (22) shows how these parameters were changing with time. Significant differences from pretreatment values are indicated by: open circles, ($p < 0.05$) and filled circles ($p < 0.01$).

1) PME/B-NTP declined significantly ($p = 0.05$) within the first 8 hours after treatment, was essentially identical at 16 hours to the pre-treatment value, but rose at 24 hours and remained slightly elevated ($p = 0.1$) through 48 hours.

2) Pi/B-NTP also declined significantly ($p = 0.05$) within the first 8 hours and remained reduced through 16 hours. By 24 hours it was not significantly different than pre-treatment.

3) PDE/B-NTP showed only a slight elevation at 16 hours and then became significantly elevated at 24 hours ($p = 0.05$) and continued to increase above pre-treatment value through 48 and 72 hours ($p = 0.01$).

4) pH as early as 8 hours post therapy had risen significantly ($p < 0.05$). This alkaline shift persisted through 16 hours, and was still growing at 48 and 72 hours.

In addition, it can be shown through the use of an F-test that the overall variance declined significantly after the first 10 Gy treatment for the NMR parameters Pi/B-NTP ($p < 0.01$), PCr/B-NTP ($p < 0.05$) and pH ($p < 0.01$). PDE/B-NTP variance increased significantly ($p < 0.05$) after the first 10 Gy treatment.

Figure 22

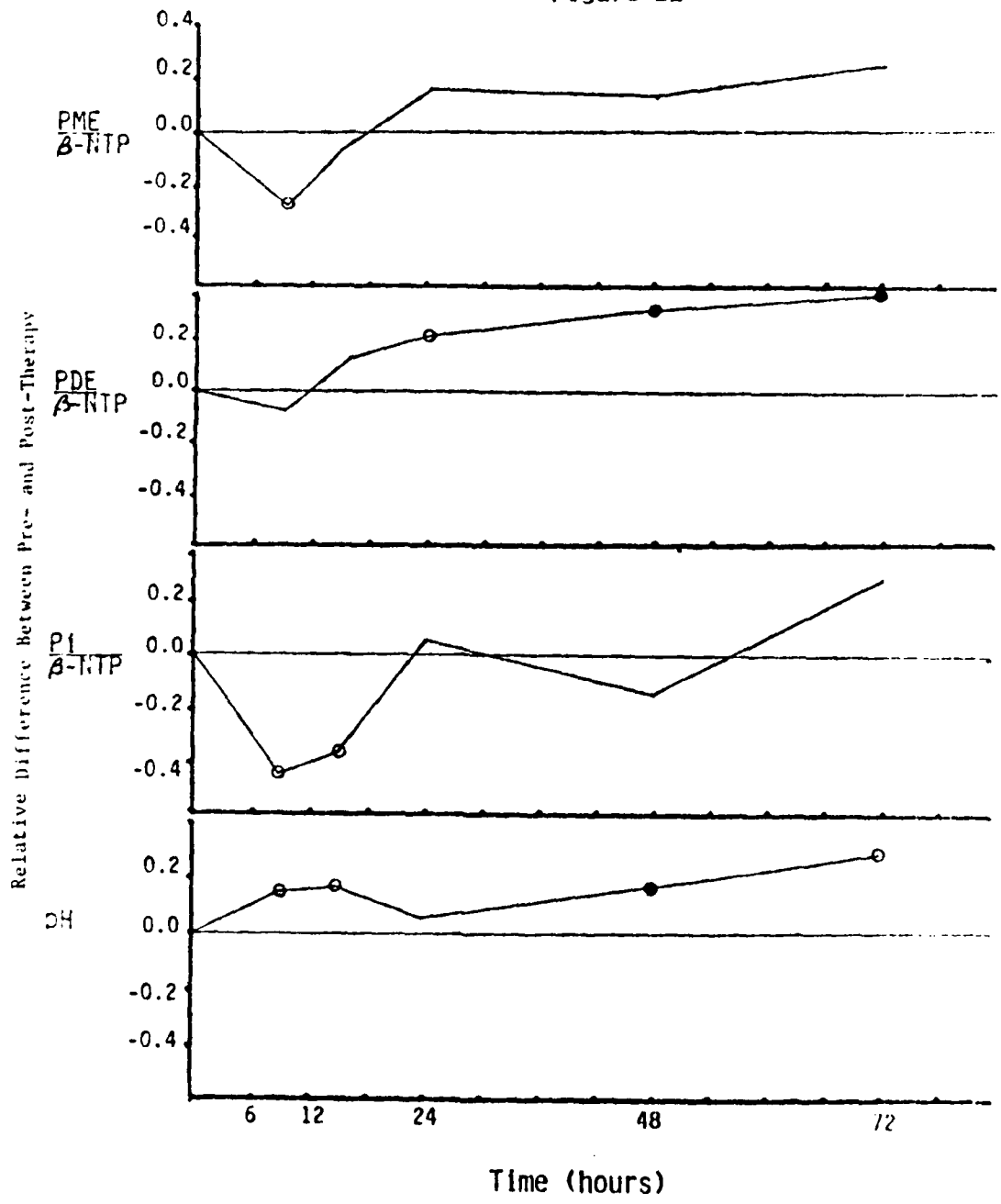

Relative Differences in NMR Parameters After Treatment with 10 Gy

The efficacy of radiation therapy at the same treatment intervals was evaluated by growth delay measurements.

Table 6

Relative Radiosensitivity
of Various Fractionation Schedules (10 Gy + 10 Gy)

Treatment Group	Area RTS (thru day 9) $x \pm \sigma$	Number of Animals
0-0	10.85 ± 3.15	10
0-8	10.65 ± 2.79	9
0-16	9.53 ± 2.31	10
0-24	11.65 ± 3.13	10
0-48	10.98 ± 2.85	17
0-72	11.73 ± 3.53	5

The time interval of 16 hours produced the lowest average RTS (i.e., the greatest radiation sensitivity). The mean area RTS for 0-16 differed from the 0-24, 0-48, and 0-72 hour treatment groups only at the $p < 0.10$ level (as determined by Student's t-test). The other time points (those less than 16 hours) were indistinguishable statistically from each other.

Clearly, as the time between fractions increased beyond 24 hours there was no enhancement to therapy.

2. Histology Patterns

Three days following a 20 Gy radiation dose, treated (n = 7) and untreated (n = 7) tumors produced on the same

animal were fixed in 10 % phosphate-buffered formalin within one minute of animal sacrifice. Fixed tumors were embedded in paraffin, and sections taken from the widest point of each tumor were stained with hematoxylin-eosin.

Treated and control slide mounts were examined and scored using a Nikon binocular compound microscope at 400x magnification. To quantify tumor micro-morphology in non-cystic regions, randomly chosen points on the microscopic field were scored for morphologic appearance after the method described by Chalkley (41). Regions underlying a total of 200 randomly distributed points per tumor (5 points in 40 different fields) were graded as necrotic, cellular, interstitial, or vascular. Necrosis was defined as the absence of an intact cellular membrane. All gradings were done with the examiner having no knowledge of the sample identity.

The results from this analysis are given in Table 7:

Table 7

Histological Determination of Necrotic Fraction in Treated (20Gy) and Untreated Tumors

Treatment Groups	Percent Necrotic Fraction $x \pm \sigma$	Number of Animals
Treated	# 0.50 ± 0.05	7
Control	0.40 ± 0.05	7

(Student's t-test: # = $p < 0.01$)

The percentage of necrotic cells was significantly greater ($p < 0.01$) in the treated tumors than in control tumors.

3. Correlation Between Radiation Sensitivity and NMR Parameters

For each of the animals described in the previous section, NMR spectra were obtained prior to any radiation therapy (i.e., pre-treatment spectra) and then again after the priming dose of radiation (i.e., post-treatment spectra). Linear regression analysis was used to compare each NMR parameter (before the first fraction or immediately prior to the second fraction) to area RTS on an individual animal basis. PCr/B-NTP was the only NMR parameter which showed a consistent sign (negative) for the slope of the regression line for all treatment intervals tested. Figure 23 relates the value of PCr/B-NTP before the first fraction ($r = -0.39$, $p < 0.01$) to average RTS for all animals. The relationship indicates that as PCr/B-NTP increases the radiation sensitivity also increases. When NMR spectra immediately before the second fraction were compared to the ultimate outcome of radiation therapy (10 + 10 Gy), PCr/B-NTP was again the only parameter to show a consistent sign for the slope for all treatment intervals tested (Figure 24). The level of correlation was essentially the same whether therapy outcome was compared

Figure 23

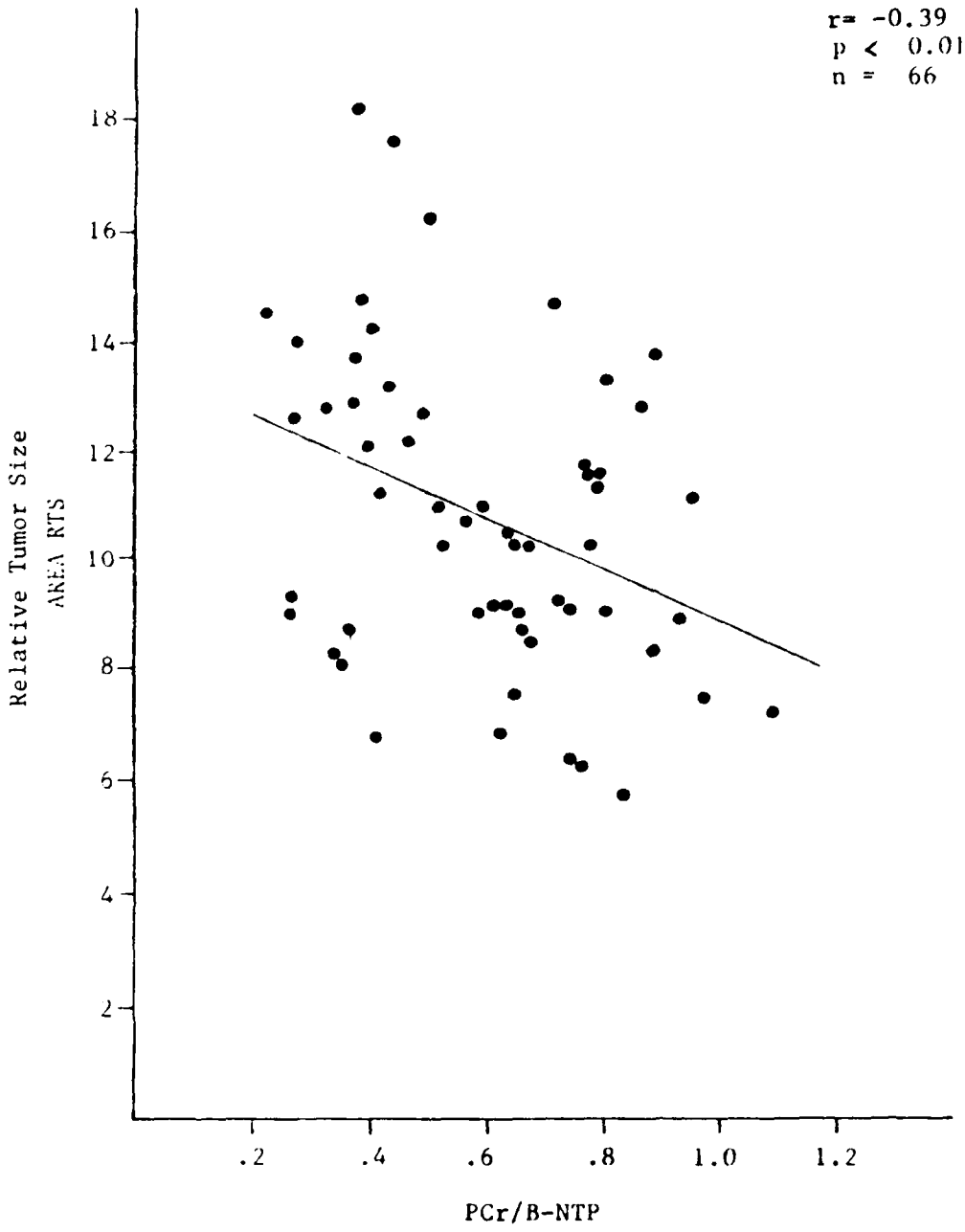

Correlation between Pre-Treatment PCr/B-NTP vs Radiation Sensitivity (10 Gy + 10 Gy)

Figure 24

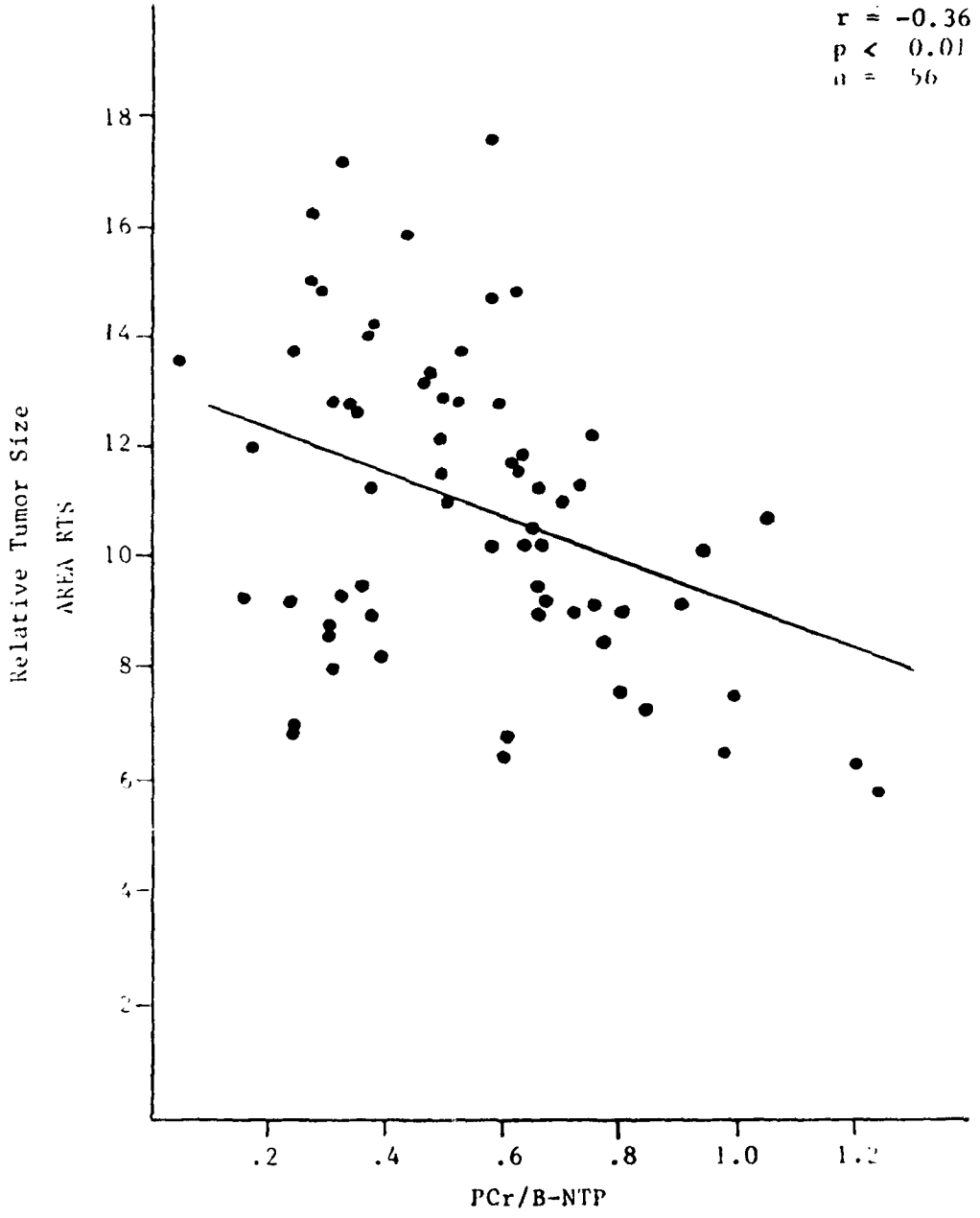

Correlation between PCr/B-NTP Prior to Second Fraction vs Radiation Sensitivity (10 Gy + 10 Gy)

with NMR values before the first fraction or before the second fraction. The correlation between treatment outcome and PCr/B-NTP was substantially higher for certain treatment groups (fraction intervals) than for the population as a whole. The pre-treatment PCr/B-NTP values were most strongly correlated with outcome for the 0-8 hour treatment interval ($r = -0.61$, $p < 0.05$, $n = 9$). Whereas, the PCr/B-NTP values at time of second fraction were most strongly correlated with outcome for a 0-24 hour fractionation schedule ($r = -0.61$, $p < 0.05$, $n = 10$).

VI. DISCUSSION

The response of individual patients to radiation therapy is highly unpredictable and considerable time can pass before the success or failure can be ascertained. Even though one of the benefits of fractionated radiation therapy is thought to be reoxygenation of the tumor, therapy fraction schedules rarely take into account the dramatic variation in reoxygenation kinetics of different tumors. A method to monitor tumor oxygen levels in patients may help predict success of radiation therapy. Information on reoxygenation could lead to development of effective therapy fraction schedules and better management of patients. The experiments described here were designed to evaluate whether 31-P NMR spectroscopy has the capability to provide information on tumor oxygenation status.

To begin we must have an understanding of what aspects of an *in vivo* tumor will contribute to the NMR spectra. A tumor is a dynamic, heterogeneous structure with at least four components. We will refer to those components as; 1) the clonogenic cell fraction, 2) the non-clonogenic cell fraction, 3) the necrotic cell fraction, and 4) the interstitial fluid.

Clonogenic cells are those cells that possess the ability to replicate indefinitely. These cells are in general less differentiated than the tumor cell population as a whole. Although clonogenic cells may be a small

percentage of the total tumor cell population for slow growing human malignancies, for the RIF-1 tumor this segment is estimated to be at least 25% of the viable cell population (26). These are the cells which will ultimately determine tumor growth and response to therapy. They represent a substantial fraction of the total tumor mass and so contribute significantly to the NMR spectra in our experimental system.

The non-clonogenic cell segment represents the remainder of the viable cell population (< 75%). We have, at present, no information about whether clonogenic cells have different 31-P NMR spectra than non-clonogenic cells.

Both segments of cells have the potential to be either fully oxygenated, partially oxygenated, or hypoxic, depending upon their proximity to their blood supply. Tumor oxygen levels have long been recognized to influence the lethal response of cells to radiation. Descher and Gray were the first to publish a curve relating radiosensitivity to oxygen tension. As the partial pressure of oxygen is increased from zero to about 30 mm Hg there is a rapid increase in radiation sensitivity. A further increase in oxygen tension to an atmosphere of pure oxygen has little, if any, further effect (13). Gray also showed that the oxygen tensions in arterial and in venous blood were both well above the 30 mm Hg level and deduced that oxygen tension would be of little importance in modifying

radiation effects in normal tissue, but that hypoxia might be a cause of radioresistance in the poorly perfused tissue of tumors. Micro-electrode measurements have shown that a large proportion of tumors have pO_2 in the range of less than 30 mm Hg (42).

In normal tissue, even a modest reduction in oxygen tension (metabolic hypoxia) results in a decline of the NMR signals for ATP and PCr. This is due to the fact that oxidative phosphorylation is the major source of ATP in most tissues. In addition to the drop in high energy phosphates a concomitant rise in low energy phosphates is observed in hypoxia. With the high levels of anaerobic glycolysis present in many tumors, it is unknown to what extent ATP and PCr can be maintained at very low oxygen concentrations in malignant tissue.

The next component in a tumor to be discussed is the necrotic fraction. Little is known about the contribution of this component to NMR spectra. However, as the cell membrane begins to break down, an increase in Pi relative to other metabolites occurs. Micro-electrode measurements indicate that regions of necrosis tend to have an alkaline pH (42).

The interstitial fluid compartment is frequently much larger in tumors than in normal tissue. The interstitial fluid in untreated RIF-1 tumors comprises about 25% of the total water present in the tumor, and this fraction can

double after cytotoxic therapy (43). The major contribution expected from this compartment to NMR spectra would be Pi, and perhaps PDE from plasma lipoproteins which leak into the tumor extravascular space.

With these four components in mind, we can begin by looking at the relationship between baseline NMR values and the consequence of radiation therapy on the natural state of the tumor. The efficacy (based on surviving fraction) of a single dose of radiation was significantly correlated with the values of two pretreatment NMR parameters. As the value of the two parameters, PCr/Pi or pH, rose the radiation sensitivity increased (reference Figures 14, and 15). Consistent with the models presented above, well oxygenated cells show an increase in high energy phosphates as represented by the ratio of PCr/Pi. Well oxygenated cells would also be expected to display a higher pH value for two reasons. First an increase in the amount of PCr is associated with an increased pH through the phosphocreatine kinase reaction. Secondly, pH is known to be affected by the levels of lactate present in the tissue. Lower levels of lactate, a by-product of anaerobic glycolysis, may be generated in better oxygenated, highly aerobic tissue. In addition, an improvement in perfusion, may improve lactate washout from the tumor. Both measures would result in an increase in pH.

Treatment of RIF-1 tumors with the drug hydralazine

(10 mg/kg) has been shown via 14-C misonidazole binding (44) to enhance tumor hypoxia. Hydralazine causes an order of magnitude decrease in radiation sensitivity of the tumor at a dose of 20 Gy (37). Hydralazine treated tumors showed the same significant correlation between PCr/Pi or pH and surviving fraction (reference Figures 16 and 17).

A drug whose effects are opposite to that of hydralazine with respect to blood flow and radiation sensitivity is the calcium antagonist flunarizine. In the KHT tumor, flunarizine (4mg/kg) caused a 30% increase in blood flow and a four fold decrease in surviving fraction (38) after treatment. Similarly, a 43% increase in blood flow was observed in the SMT-2A tumor in rats by Kaelin, et al. (45).

Before investigating any correlation between NMR values and radiation sensitivity resulting from drug-treated tumors, the NMR spectra had to be characterized. The hydralazine spectral changes were rapid (noticeable within 15 minutes). The spectra continued to change throughout the first hour, showing a dramatic increase in Pi and an equally dramatic decline in high energy phosphates. In contrast to the NMR time course, the radiobiologic effects of hydralazine are already maximal immediately after administration. This can be shown both for radiation sensitivity and for drugs such as RSU 10-69 and Mitomycin C which are specifically targeted to hypoxic cells (37).

Since the radiobiologically significant hypoxia is maximal within a few minutes (37), while the NMR spectral changes observed were not, it appears that the tumor can maintain ATP and PCr levels for a short period of time on the anaerobic metabolism of the glucose reserves.

Probably because the untreated RIF-1 tumor is so well oxygenated, the blood flow changes produced by flunarizine are less dramatic than for hydralazine. The major changes with time were a significant decline in Pi followed by an increase in PCr. An interesting feature caused by flunarizine was a clear split in the Pi resonance with an appearance of a new alkaline compartment which increased with time (Figure 19). This may indicate an anatomical heterogeneity within the tumor, perhaps reflecting either an unequal drug delivery or drug response. A less likely explanation is a drug-induced shift in Pi from extra- to intra-cellular if there is a steep pH gradient across the cell membrane.

Clearly the 31-P spectra do reveal changes in tumor energy levels following drug treatment consistent with the previously reported changes in tumor blood flow and radiobiologic hypoxia. These apparent differences in tumor oxygenation were associated with alterations in radiation sensitivity when tumors were irradiated after drug treatment. As expected the flunarizine treated tumors were statistically more radiation sensitive than those treated

with hydralazine (reference table 3).

Another class of compounds known to have effects on both tumor blood flow and radiation sensitivity are anesthetics. Treatment of mice bearing EMT6 tumors with sodium pentobarbital caused a 10°C drop in tumor temperature and an decrease in radiation sensitivity suggesting that tumor perfusion had been depressed (40). Tumor blood flow in KHT tumors, as measured by 131-Xenon washout, fell 50% following administration of PB and produced an increase in tumor hypoxic cell fraction (39).

The increased levels of hypoxia induced in RIF-1 tumors by pentobarbital were visible in the 31-P NMR spectrum. Although pentobarbital treated animals could not be compared to unanesthetized animals in the NMR spectrometer, we did compare the effects of pentobarbital to the milder anesthetic combination of Ketamine/Acepromazine.

Mean spectral resonances for RIF-1 tumors in KA treated mice were found to be significantly different from PB. Twenty minutes after administration of PB the Pi resonant peaks was significantly higher (relative to any other spectral resonance) than was observed when KA was administered (reference Table 4). In addition the variance for NMR parameter values was significantly higher for PB treated animals than for KA. The elevated levels of Pi in the PB tumors was associated with a slightly higher level of radiation resistance as indicated by the growth delay

assay (reference Figure 21). Other studies currently in progress have shown in vivo by near infrared spectroscopy a reduction in total tumor oxyhemoglobin in RIF-1 following administration of PB, which was not seen after KA anesthesia (46).

From these data it is clear that under a variety of conditions both values of pH and PCr/Pi as measured in the tumor before radiation treatment are associated with the efficacy of single fraction radiation therapy. These correlations were strong enough to support the hypothesis that NMR parameters reflect tissue oxygenation level. This lead us to evaluate the ability of NMR to monitor the process of reoxygenation in fractionated radiation therapy.

The term reoxygenation denotes the reacquisition of radiosensitivity by those cells that were able to survive irradiation because they were hypoxic at the time of exposure. The RIF-1 tumor has been shown to reoxygenate rapidly (28) with the hypoxic fraction dropping to 50% within the first hour, and was essentially complete within 24 hours. Previous NMR studies (22) have failed to examine the tumor during this critical period of reoxygenation.

Immediately following irradiation, the cellular compartments of the tumor will not only be different from pre-treatment condition, but will be changing. The previously well oxygenated cells, which were disproportionatly subjected to the lethal effects of radiation, will be

dying. This will dramatically reduce the competition for the oxygen supply, allowing the previously hypoxic, quiescent cells to re-enter the cell cycle. There will be a gradual increase in tumor necrosis if the rate of cell death exceeds cell clearance, and consequently an increase in the interstitial fluid.

These changes in cellular compartments will contribute to the changes we observe in the post treatment NMR spectra. No indication of acute (8 hour) metabolic injury from the radiation (increased Pi or decreased PCr) was observed in the NMR spectra. On the contrary, by 8 hours there was a significant decline in Pi relative to NTP (reference Table 5). This is consistent with an increase in the available oxygen within the tissue although the exact mechanism is undetermined. In previous studies, a similar decline in Pi/B-NTP was shown to have a greater magnitude and duration with increasing radiation dose (22). The other NMR parameter that showed a significant change in the early time points was tumor pH. The observed increase in tumor pH was also consistent with an improved energy state of the tumor due to reduced lactate production. Increases in necrosis which might also cause increased pH are unlikely at this early time point. Unlike the Pi/B-NTP decline which only persisted through 16 hours, the pH continued to rise through the 72 hour time point. Although these same changes in Pi/B-NTP and pH have been seen, in

previous experiments, at later time points after irradiation, this was the first study to show changes in the early time course associated with reoxygenation.

Significant elevation of PDE/B-NTP was not observed until 24 hours after treatment. PDE resonances in _in vivo_ spectra may arise from both the phospholipid metabolites GPE and GPC, or from intact but highly mobile phospholipids. PCA extract studies will be required to determine the nature of the PDE compounds which increase after radiation therapy. Increases in GPC and GPE could be associated with increased cell membrane degradation and necrosis. With a cell cycle time of 17 hours for RIF-1 tumor cells, this PDE increase is consistent with the eventual cell death following irradiation. In addition, increases in phosphodiester due to plasma lipoproteins have also been associated with an inflammatory response (47). Either or both of these mechanisms may be operating to result in the observed PDE increase.

Histological analysis of tumors 72 hours after 20 Gy irradiation showed clear evidence of cell lysis and increased necrosis relative to sham treated controls (reference Table 7). This is in line with the proposed mechanisms for PDE elevation. Also, as mentioned earlier, elevated pH values have been observed in regions of tumor necrosis consistent with our findings of significant elevation of pH through 72 hours.

Even though changes in NMR parameters could be identified at various time points after a priming dose of radiation (10 Gy), no significant improvement in treatment efficacy was observed when a second 10 Gy fraction was delivered at any of the time points examined (0 to 72 hours). The Area RTS from animals treated on the 0-16 hour fractionated schedule showed a small improvement ($p < 0.10$) compared to the longer fractionation intervals. This may indicate that tumor growth between fractions is over-riding any gains from reoxygenation. The inability to show an improvement in therapy outcome between treatment groups could be due to the high level of animal variability which was observed, even in this population of syngeneic mice.

When the NMR parameters were evaluated on an individual animal basis it could be shown that the value of PCr/B-NTP was significantly correlated with the outcome of fractionated therapy (reference Figure 23). PCr is the highest energy compound found within a cell, and the most sensitive to oxygen reduction in heart and brain tissue (7). Thus it is not surprising that PCr/B-NTP should be the best predictor of fractionated radiation therapy. The degree of correlation between treatment outcome and the value of PCr/B-NTP at the time of second fraction was essentially the same as the degree of correlation with the pre-treatment value (reference Figure 24).

It is interesting that parameters that predicted

outcome for single fraction therapy (pH and PCr/Pi) were not identical to that found to correlate to multi-fraction therapy (PCr/B-NTP) This may indicate that some other factor in addition to oxygenation, perhaps proliferation, is important in determining the outcome of single fraction radiotherapy.

VII. CONCLUSIONS

Three salient points were revealed by this work. First, from the single fraction experiments, NMR values were clearly shown to be related to tumor hypoxia and radiation sensitivity. Second, in the fractionated dose experiments it was possible to show significant changes in NMR values within 8 hours after radiation therapy. The nature of these changes (a decline in Pi and an increase in pH) is consistent with the process of reoxygenation. Third, no single time interval was shown to be optimal for all animals. Instead, the value of PCr/B-NTP was correlated on an individual animal basis with the ultimate outcome of radiation therapy. Of particular interest was the fact that the value of PCr/B-NTP as determined via 31-P NMR spectroscopy was equally capable of forecasting radiosensitivity at both pre-treatment and at the time of the second fraction.

These results are encouraging enough to recommend further study. Specifically another tumor line should be selected which is known to be less well-oxygenated, so that the relative changes induced by radiation therapy will be more pronounced. A good candidate for this would be the EMT-6/SF (49) with a hypoxic fraction in the untreated state of 20%.

Additional study is also recommended since informal clinical studies using the technique of 31-P NMR Spectro-

scopy to optimize radiation therapy are already underway (50).

VIII. BIBLIOGRAPHY

1. Thomlinson, R. H. Reoxygenation Kinetics in Experimental Rodent Tumors. Carmel Conference on Time and Dose Relationships in Radiation Biology as Applied to Radiotherapy (Proceedings), p. 242, 1969.

2. Peters, L. J., Withers, H. R., Thames, H. D., and Fletcher, G. H. The problem: tumor radioresistance in clinical radiotherapy. in: Biological Bases and Clinical Implications of Tumor radioresistance. (Fletcher, G. H., Nervi, C., Withers, H. R., Arcangeli, G., Mauro, F., and Tapley, N. duV., eds) New York, NY: Masson Publishing USA, Inc., pp.101-108.

3. Evanochko W. T., Ng, T. C., Lilly, M. B., Lawson, A. J., Corbett, T. H., Durant, J. R., and Glickson, J. D. In vivo ^{31}P NMR study of the metabolism of murine mammary 16/C adenocarcinoma and its response to chemotherapy, x-radiation, and hyperthermia. Proc. Natl. Acad. Sci. USA, 80: 334-338, 1983.

4. Wehrle, J. P., Li, S.-J., Rajan, S. S., Steen, R. G., and Glickson, J. D. ^{31}P and ^{1}H NMR spectroscopy of tumors in vivo: Untreated growth and response to chemotherapy. Ann. N. Y. Acad. Sci., 508: 200-215, 1987.

5. Ackerman, J. J. H., Grove, T.H., Wong, G. G., Gadian, D. G., and Radda, G. K. Mapping of metabolites in whole animals by ^{31}P NMR using surface coils. Nature. 283:167-170, 1980.

6. Hoult, D. I., Busby, S. J. W., Gadian, D. G., Radda, G. K., Richards, R. E., and Seeley, P. J. Observations of tissue metabolism using phosphorus 31 nuclear magnetic resonance. Nature: 252:285-287, 1974.

7. Prichard, J. W., and Shulman, R. G. NMR spectroscopy of brain metabolism in vivo. Ann. Rev. Neurosci., 9:61-85, 1986.

8. Evelhoch, J. L., Sapareto, S. A., Nussbaum, G. H., and Ackerman, J. J. H. Correlations between ^{31}P NMR spectroscopy and ^{15}O perfusion measurements in the RIF-1 murine tumor in vivo. Radiat. Res. 106: 121-132, 1986

9. Cohen, J. S., Lyon, R. C., Chen, C., Faustino, P. J., Batist, G., Shoemaker, M., Rubalcaba, E., and Cowan, K. H. Differences in phosphate metabolite levels in drug-sensitive and -resistant human breast cancer cell lines determined by 31-P magnetic resonance. Cancer Res., 46: 4087-4090, 1986.

10. Ng, T. C., Evanochko, W. T., Hiramoto, R. N., Ghanta, V. K., Lilly, M. B., Lawson, A. J., Corbett, T. H., Durant, J. R., and Glickson, J. D. ^{31}P NMR spectroscopy of in vivo tumors. J. Magn. Reson., 49: 271-286, 1982.

11. Evanochko, W. T., Ng, T. C., and Glickson, J. D. Application of in vivo NMR spectroscopy to cancer. Magn. Reson. Med., 1: 508-534, 1984.

12. Steen, G. R., Tamargo, R. J., Rajan, S. S., McGovern, K. A., Brem, H., Wehrle, J. P., and Glickson, J. D. In vivo ^{31}P NMR Spectroscopy of subcutaneous 9L gliosarcoma: Effects of tumor growth and treatment with 1,3-Bis(2-chloroethyl)-1-nitrosourea on tumor bioenergetics and histology. Cancer Res., 48: 676-681, 1988.

13. Hall, E. J. Solid tumor systems and reoxygenation. in: Radiobiology for the Radiologist, Second Edition. Philadelphia, PA: Harper and Row, Publishers, Inc., pp. 217-244, 1978.

14. Sutherland, R. M., and Franko, A. J. On the nature of the radiobiologically hypoxic fraction in tumors. Int. J. Radiat. Oncol. Biol. Phys., 6: 117-120, 1980.

15. Okunieff, P. G., Koutcher, J. A., Gerweck, L., McFarland, E., Hitzig, B., Urano, M., Brady, T., Neuringer, L., Suit, H. D. Tumor size dependent changes in a murine fibrosarcoma: Use of in vivo ^{31}P NMR for non-invasive evaluation of tumor metabolic state. Int. J. Radiat. Oncol. Biol. Phys., 12: 793-799 1986.

16. Maris, J. M., Evans, A. E., McLaughlin, A. C., D'Angio, G. J., Bolinger, L., Manos, H., and Chance, B. ^{31}P Nuclear magnetic resonance spectroscopic investigations of human heuroblastoma in situ. New England J. Med., 312: 1500-1505, 1985.

17. Gyulai, L., Bolinger, L., Leigh, J. S., Jr., Barlow, C., and Chance, B. Phosphorylethanolamine-the major constituent of the phosphomonoester peak observed by ^{31}P-NMR on developing dog brain. FEBS Lett. 178: 137-142, 1984.

18. Onodera, K., Okuba, A., Yasumoto, K., Suzuki, T., Kimura, G., and Nomoto, K. ^{31}P Nuclear magnetic resonance analysis of lung cancer: the perchloric acid extract spectrum. Jpn. J. Cancer Res. (Gann) 77: 1201-1206, 1986.

19. Oberhaensli, R. D., Bore, P. J., Rampling, R. P., Hilton-Jones, D., Hands, L. J., and Radda, G. K. Biochemical investigation of human tumors in vivo with phosphorus-31 magnetic resonance spectroscopy, Lancet, 2: 8-11, 1986.

20. Li, S.-J., Wehrle, J. P., Rajan, S. S., Steen, R. G., and Glickson, J. D. Response of mouse radiation-induced fibrosarcoma-1 to cyclophosphaamide monitored by n31P nuclear magnetic resonance spectroscopy. Cancer Res. (in press.)

21. Li, S.-J., Wehrle, J. P., and Glickson, J. D. (unpublished results).

22. Rajan, S. S., Wehrle, J. P., Li, S.-J., Steen, R. G., and Glickson, J. D. Bioenergetic Changes in Radiation-induced Fibrosarcoma-1 after radiation therapy monitored by ^{31}P NMR spectroscopy., submitted for publication.

23. Koutcher, J. A., Okunieff, P., Neuringer, L., Suit, H., and Brady, T. Size dependent changes in tumor phosphate metabolism after radiation therapy as detected by ^{31}P NMR spectroscopy. Int. J. Radiat. Oncol. Biol. Phys., 13: 1851-1855, 1987.

24. Sijens, P. E., Bovve, W. M. M. J., Seijkens, D., Los, G., and Rutgers, D. H. In vivo ^{31}P-nuclear magnetic resonance study of the response of a murine mammary tumor to different doses of γ-radiation. Cancer Res., 46: 1427-1432, 1986.

25. Bhujwalla, Z., Maxwell, R. J., Tozer, G. M., and Griffiths, J. R. The significance of changes in ^{31}P magnetic resonance spectra following radiotherapy in mouse tumors. Soc. Magn. Reson. Med. (Abs). 2: 975, 1987.

26. Twentyman, P. R., Brown, J. M., Gray, J. W., Franko, A., Scoles, M. A., and Kallman, R. F. A new mouse tumor model system (RIF-1) for comparison of endpoint studies. J. Natl. Cancer Inst., 64: 595-604, 1980.

27. Evanochko, W. T., Ng, T. C., Glickson, J. D., Durant, J. R., and Corbett, T. H. Human tumors as examined by in vivo ^{31}P NMR in athymic nude mice. Biochem. Biophys. Res. Commun. 109:1346-1351, 1982.

28. Dorie, M. J. and Kallman, R. F. Reoxygenation in the RIF-1 tumor. Int. J. Radiat. Oncol. Biol. Phys., 10: 687-693, 1984.

29. Brown, J. M. Evidence for acutely hypoxic cells in mouse tumors and a possible mechanism for reoxygenation. Br. J. Radiol. 52: 650-656, 1979.

30. Rajan, S.S., Wehrle, J.P., and Glickson, J.D. A novel double tuned circuit for in vivo NMR. J. Magn. Reson., 74: 147-154, 1987.

31. Evanochko, W. T., Sakai, T. T., Ng, T. C., Krishna, N. R., Kim, H. D., Zeidler, R. B., Ghanta, V. K., Brockman, R. W., Schiffer, L. M., Braunschweiger, P. G., and Glickson, J. D. NMR study of in vivo RIF-1 tumors: analysis of perchloric acid extracts and identification of ^{1}H, ^{31}P and ^{13}C resonances. Biochim. Biophys. Acta, 805: 104-116, 1984.

32. Moon, R. B., and Richards, J. H. Determination of Intracellular pH by ^{31}P Magnetic Resonance. J. Biol. Chem., 246: 7276-7278.

33. White, D. R. Tissue substitutes in experimental radiation physics. Med. Phys., 5:472-473, 1978.

34. Lesser, M. L., Braun, H. I., and Helsor, L. Statistical methods for comparing treatment efficacies; Applications to nude mice experimentation. Expl. Cell Biol. 48: 126-137, 1980.

35. Hirst, D. G., Hazlehurst, J. L., and Brown, J. M. Changes in misonidazole binding with hypoxic fraction in mouse tumors. Int. J. Radiat. Oncol. Biol. Phys. 11: 1349-1355.

36. Stratford, I. J., Godden, J., Howells, N., Embling, P., and Adams, G. E. Manipulation of tumor oxygenation by hydralazine increases the potency of bioreductive radiosensitizers and enhances the effect of melphalan. Int. Congress Radiat. Res. (Proceedings) 2: 737-742, 1987.

37. Chaplin, D. J. Hypoxia-targeted Chemotherapy: A role for vasoactive drugs. Int. Congress Radiat. Res. (Proceedings) 2: 731-736, 1987.

38. Hill, R. P., and Stirling, D. Oxygen delivery and tumor response. Int. Congress Radiat. Res. (Proceedings) 2: 725-730, 1987.

39. Pallavicini, M. G., and Hill, R. P. Tumor blood flow and radiosensitivity in the murine KHT tumor. Int. J. Radiat. Oncol. Biol. Phys. 9: 1321-1326, 1974.

40. Rockwell, S., and Loomis, R. Effects of sodium pentobarbital on the radiation response of EMT6 cells in vitro and EMT6 tumors in vivo. Radiat. Res. 81: 292-302, 1980.

41. Chalkley, H. W. Method for quantitative morphologic analysis of tissues. J. Natl. Cancer Inst. 4: 47-53, 1943.

42. Vaupel, P. W., Frinak, S., and Bicher, H. I. Heterogeneous oxygen partial pressure and pH distribution in C3H mouse mammary adenocarcinoma. Cancer Res. 41: 2008-2013, 1981.

43. Braunschweiger, P. B., Schiffer, L. M., and Furmanski, P. ^{1}H-NMR Relaxation times and water compartmentalization in experimental tumor models. Magn. Reson. Imaging, 4: 335-342, 1986.

44. Brown, J. M. Exploitation of bioreductive agents with vasoactive drugs. Int. Congress Radiat. Res. (Proceedings) 2: 719-724, 1987.

45. Kaelin, W. G., Jr., Shrivastav, S., and Jirtle, R. L. Blood flow to primary tumors and lymph node metastases in SMT-2A tumor-bearing rats following intravenous flunarizine. Cancer Res. 44: 896-899, 1984.

46. Steen, R. G., Wilson, D. A., Bowser, C., Rajan, S. S., Wehrle, and Glickson, J. D., unpublished results.

47. Raymond, T. L., and Reynolds, S. A. Lipoprotein metabolism in the extravascular space. Inflammation 7: 241-246, 1983.

48. Thames, H. D., Jr., Peters, L. J., Withers, H. D., and Fletcher, G. H. Accelerated fractionation vs hyperfractionation: rationales for several treatments per day. Int. J. Radiat. Oncol. Biol. Phys. 9: 127-138.

49. Begg, A. C., Fu, K. K., Kane, L. J., and Phillips, T. L. Single-agent chemotherapy of a solid murine tumor assayed by growth delay and cell suvival. Cancer Res. 40: 145-154, 1980.

50. Ng, T. C., Vijayakumar, S., Majors, A. W., Thomas, F. J., Meany, T. F., and Baldwin, N. J. Response of a non-Hodgkin lymphoma to ^{60}Co therapy monitored by ^{31}P MRS in situ. Int. J. Radiat. Oncol. Biol. Phys. 13: 1545-1551, 1987.

CURRICULUM VITAE

CINDY L. BOWSER, CAPTAIN, USAF, BSC

The Johns Hopkins Medical Center

School of Hygiene and Public Health

Department of Environmental Health Sciences

Division of Radiation Health Sciences
600 N. Wolfe Street
Baltimore, Maryland 21205
(301) 955-3350

EDUCATION:

Master of Science in Hygiene, University of Pittsburgh School of Public Health, Department of Radiation Health, Pittsburgh, Pennsylvania, 1981. Concentration in Health Physics.

Bachelor of Science, Grove City College Grove City, Pennsylvania, 1980. Major in Chemistry.

PROFESSIONAL EXPERIENCE:

Field Surveyor, Department of Energy Fellowship Cannonnsburg, Pennsylvania, 1980-1981.

Radiation Health Physicist, School of Aerospace Medicine Radiation Sciences Division, Radiation Biology Branch, Brooks Air Force Base, San Antonio, Texas, 1981-1984.

Radiation Safety Officer, Wilford HAll Medical Center Department of Radiology, Medical Phsyics Service, Lackland Air Force Base, San Antonio, Texas, 1984-1985.

PROFESSIONAL AFFILIATIONS:

Member, Health Physics Society.

Member, Air Force Association.

AWARDS:

1976, Cooper Energy Service Scholarship.

1984, United States Air Force Commendation Medal.

1985, United States Air Force Commendation Medal (First Oakleaf Cluster).

1988, United States Air Force Achievement Medal.

PERSONAL DATA:

[redacted]

Citizenship: United States of America

[redacted]

Marital Status: Single, no children

[redacted]